Journal of Physics: Condensed Matter

OPEN ACCESS

RECEIVED
30 April 2026

REVISED
3 August 2026

ACCEPTED FOR PUBLICATION
2 September 2026

PUBLISHED
15 September 2026

TOPICAL REVIEW

Ultrafast charge and energy transfer dynamics in solids and at interfaces revealed by time-resolved x-ray absorption spectroscopy

A Eschenlohr*

Faculty of Physics and Center for Nanointegration Duisburg-Essen (CENIDE), University of Duisburg-Essen, Lotharstr. 1, 47057 Duisburg, Germany

* Author to whom any correspondence should be addressed.

E-mail: andrea.eschenlohr@uni-due.de

Keywords: x-ray absorption spectroscopy, ultrafast dynamics, pump-probe method, time-resolved x-ray spectroscopy

Abstract

The excitation of solid materials with femtosecond optical pulses induces non-equilibrium states that are interesting for both fundamental and application-related reasons, as their properties can be quite different from those generated by e.g. thermal excitation or chemical doping. However, once several degrees of freedom such as electronic and lattice excitations, or multiple components in a heterostructure, couple strongly, analyzing the resulting ultrafast dynamics on femto- to picoseconds requires element-sensitive spectroscopy on these timescales. This Topical Review discusses how new insights into ultrafast charge and energy transfer dynamics in solids and at interfaces can be gained from time-resolved soft x-ray absorption spectroscopy (XAS). The state-of-the-art of the pump-probe XAS method at large scale facilities, namely synchrotron Femtoslicing sources and x-ray free electron lasers, is reviewed, with an emphasis on the opportunities and challenges of the respective facilities that motivate new methodological developments. For three selected material systems, it is then shown how XAS with femtosecond time resolution, in conjunction with theoretical calculations, is able to reveal and characterize non-equilibrium states by analyzing the transient electronic structure as well as lattice excitation via characteristic, time-dependent spectral features. Finally, future opportunities through the further development of laboratory-based soft x-ray sources and the combination of time-resolution with non-linear XAS are presented.

1. Introduction

Gaining insight into electronic, spin and lattice excitations in solids is interesting not only from the standpoint of fundamental science, but the development and optimization of technological applications as well. Understanding the excitation, transport and relaxation of charge carriers is highly relevant for electronics, spintronics, catalysis and photovoltaics, to mention just a few examples. Most devices are based on heterostructures, where two or more solid layers of different materials are combined. In heterostructures, charge, spin and energy transfer processes occur at interfaces, which determines functionality but also increases the degrees of freedom that need to be considered.

The fundamental timescales of these processes lie in the femtosecond (fs) to picosecond (ps) time range. For example, electronic lifetimes in transition metals are in the range of a few fs to some tens of fs for energies close to the Fermi level [1]. Charge transport in the ballistic range proceeds with velocities on the order of nm fs^{-1} [2–4]. In ferromagnetically ordered metals, electron lifetimes and charge transport become spin-dependent [2, 4, 5]. The resulting superdiffusive spin transport has been identified as one origin of the ultrafast demagnetization of metallic ferromagnets [4, 5], which occurs on several 100 fs timescales [6], together with spin-flip scattering mediated by spin–orbit coupling [7, 8]. Electron–phonon coupling subsequently leads to energy transfer from optically excited electrons to the

lattice within few hundreds of fs to several ps [9]. Consequently, accessing these processes experimentally relies on pump-probe techniques using optical, x-ray or electron pulses with correspondingly ultrashort durations as probes.

Since femtosecond ultrashort pulsed optical lasers became available, close to four decades of successful experiments unraveling these ultrafast processes in the time domain have been performed. These advances have been achieved through methodological developments in different pump-probe experiments such as, for example, transient optical absorption spectroscopy, time-resolved (tr) non-linear optical spectroscopy including (magnetization-induced) second harmonic generation (SHG) and two-photon photoemission spectroscopy. With ultrashort pulsed electron, hard and soft x-ray sources, ultrafast electron and x-ray diffraction as well as time-resolved x-ray absorption spectroscopy (XAS) and x-ray magnetic circular dichroism (XMCD) have further been developed. These experimental advances have gone hand in hand with theoretical developments. Applicable methods range from comparably simple rate equation models [10, 11] or other model-based approaches to atomistic simulations and ab initio methods like time-dependent density functional theory (TDDFT) [7].

At the core of experiments performed in the time domain lies the classification of different microscopic processes according to their timescales or corresponding rates of change. Electronic and spin excitations are often separated from excitations involving the movement of the ion cores, i.e. phonons, via different characteristic timescales [6]. The two-temperature model (2TM) [10] and its extension to spin dynamics, the three-temperature model [11], are frequently employed for this purpose. However, these models rely on two fundamental assumptions, namely that the different baths representing the electron, lattice and spin temperatures are in internal thermal equilibrium, and that coupling between two of those baths involves a single coupling constant. One or both of these assumptions might in fact not be met: For example, lattice excitations are often assumed to be thermal, in the sense that they can be described by one common lattice temperature. However, it has been shown that equilibration between phonon modes can take several 10 ps even in relatively simple materials like the transition metal Ni [12]. Preferential interaction of optically excited charge carriers with so-called strongly coupled optical phonons in oxides or two-dimensional materials [13] is a further source of phonon non-equilibrium.

This motivates the use of spectroscopic information in the domain of frequency (or wavelength or photon energy) in time-resolved experiments. Competing interactions can thus potentially be separated by their different spectral signatures. Furthermore, spectroscopic observables that are specific to surfaces or interfaces, or to different components in a heterostructure, via interface-sensitivity respectively element-sensitivity are highly desired. Thereby, coupling of excitations across interfaces as well as the occurrence of new electronic, magnetic and/or vibrational properties due to hybridization at the interfaces of heterostructures can be resolved. Another aspect are materials exhibiting strong electronic correlations. In some of these materials, the optical excitation of novel, 'hidden' long-living or metastable states has been predicted or observed [14, 15]. This again motivates spectroscopic techniques which are sensitive to the influence of electronic correlations under non-equilibrium conditions.

Pump-probe XAS with femtosecond time resolution is a technique which provides this spectroscopic information for non-equilibrium states. Ultrafast changes to the electronic population as well as the electronic structure itself, induced by optical excitation, are probed through resonant x-ray absorption. The x-ray absorption spectra exhibit characteristic transient modifications that can be linked to the excitation of different degrees of freedom, namely the electron charge and spin as well as the crystal lattice, through their transient spectral shape. As will be demonstrated in this Topical Review for a range of material systems, transient spectral shifts allow to identify correlation-induced modifications of the electronic structure, while broadening is associated with electron repopulation or lattice excitation, depending on the timescale. In this way, charge and energy transfer can be tracked by means of combined time domain and spectroscopic information in pump-probe XAS at large scale x-ray sources, see figure 1.

In this Topical Review, I will briefly review the strengths of XAS for the characterization of the thermal ground state and its application in optical pump, XAS probe experiments at large scale facilities that provide fs x-ray pulses in section 2. An overview over previous work probing electronic, spin and lattice excitations with time-resolved XAS will be given in section 3. Then I will describe for selected current examples how pump-probe XAS with fs time resolution reveals new insights into charge and energy transfer dynamics in section 4 before concluding in section 5 and giving a short outlook on future possibilities in section 6.

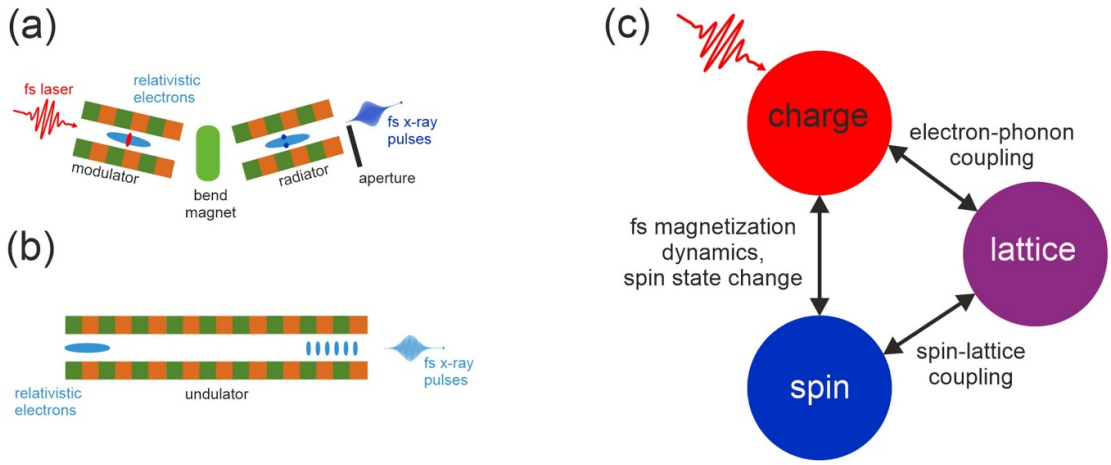

Figure 1. (a) Schematic depiction of generation of fs x-ray pulses at a synchrotron-based Femtoslicing facility. Interaction of an intense fs laser pulse with a ps electron pulse in a first undulator (modulator) leads to energy modulation of a small 'slice' of the electrons, which are then spatially offset in a subsequent bend magnet and produce fs x-ray pulses in a second undulator (radiator). (b) Schematic depiction of generation of fs x-ray pulses at an x-ray free electron laser. During propagation through a very long undulator, the SASE process leads to microbunching of the electron pulses and thus coherent radiation of very intense x-rays. (c) Charge, spin and lattice degrees of freedom in solids with their respective coupling processes (depicted by double-headed arrows), after the electronic structure is excited through absorption of the pump pulse.

2. Time-resolved XAS method

2.1. Ground state XAS

XAS is an established method for the characterization of materials in the ground state, i.e. thermal equilibrium [16–18]. With polarization control of x-rays, dichroism can be exploited to also investigate ferro-, ferri- or altermagnetic order via XMCD [19, 20] and antiferromagnetic order via x-ray magnetic linear dichroism (XMLD) [19]. This Topical Review focuses on resonant absorption of linearly polarized x-rays in the soft x-ray range (100–2000 eV photon energy), which includes the *K* edge of oxygen, the *L* edges of transition metals and the *M* edges of rare earths. The soft x-ray range thus covers transition metal and rare earth ferromagnets as well as transition metal oxides. The corresponding core level to valence transitions are from 1*s* to 2*p* states for the *K* edge, from 2*p* to 3*d* states for the L_{23} edges and from 3*d* to 4*f* states for the M_{45} edges. The energies of these transitions are element-specific. XAS thus provides element- and orbital-sensitivity. Moreover, XAS is a local probe, as it involves the generation of a core-hole (core-hole exciton). Therefore, it can be applied to amorphous materials and does not require crystallinity or long-range order. XAS probes unoccupied electronic states, or more precisely the unoccupied electronic density of states (DOS) modified by the presence of the core hole. Soft x-ray XAS is typically measured with monochromatic x-rays that are transmitted through or reflected from the sample. Alternatively, the absorbed x-ray intensity is detected via total or partial electron yield. XAS in transmission geometry measures bulk or thin film properties while electron yield and reflectivity in grazing incidence provide surface sensitivity due to limited x-ray penetration respectively electron escape depth. XAS can roughly be divided into the near-edge x-ray absorption fine structure (NEXAFS) compared to extended x-ray absorption fine structure (EXAFS) [21]. Here, I will mostly restrict myself to discussing NEXAFS. NEXAFS is also termed x-ray absorption near edge structure (XANES), in particular in the hard x-ray range.

2.2. Pump-probe XAS

Pump-probe experiments are conducted as stroboscopic measurements, in which an initial, strong pulse excites the sample in order to induce a non-equilibrium state, and a second, weaker pulse probes the resulting change to the sample's properties at a well-defined time delay. In the case of tr-XAS experiments, the pump pulse is typically a femtosecond laser pulse in the infrared, visible or ultraviolet range. Such stroboscopic experiments require that the detection is gated to a specific x-ray pulse, not the entire pulse train produced by the electron storage ring or FEL. Therefore, in tr-XAS photons are usually detected, in contrast to total or partial electron yield common in static XAS. X-ray photon detection can be performed in transmission or reflection geometry, or alternatively fluorescence is detected. A drawback of reflection geometry is the extremely low reflectivity of solid surfaces in the soft x-ray range even

under grazing incidence, which limits the number of detected photons and thus the achievable signal-to-noise ratio. Transmission geometry requires thin film samples that are freestanding or prepared on a substrate that is thin enough to be transparent for soft x-rays, which imposes constraints on the type of materials that can be studied, or their quality (e.g. crystallinity).

At synchrotrons, pump-probe experiments with ps time resolution employ the native pulse duration of several tens of ps to ns as well as the so-called low-alpha mode with few ps to 10 ps x-ray pulses. Shortening the x-ray pulse duration is achieved through the Femtoslicing method, which will be discussed in section 2.3.1. X-ray free electron lasers (XFELs) based on linear accelerators will be discussed in section 2.3.2, while the outlook in section 6.1 introduces laboratory-based sources.

2.3. Large scale facilities

Femtosecond time-resolved XAS requires correspondingly short x-ray pulses. While laboratory-based sources are increasingly becoming available and start to reach the soft x-ray range, as will be discussed in section 6, large scale facilities remain the primary sources to deliver tunable fs x-ray pulses. The following sections will present two different approaches that each offer specific opportunities and challenges, namely Femtoslicing sources at synchrotrons and XFELs.

2.3.1. Synchrotron femtoslicing sources

Synchrotron radiation sources provide x-ray pulses with native durations of about 70 ps to ns. With the so-called femtosecond slicing or Femtoslicing technique, much shorter x-ray pulses can be generated for use in pump-probe XAS experiments. The working principle is the following, see figure 1(a): A high intensity fs laser pulse interacts with the ps electron bunch in an insertion device (undulator). When laser and electron bunch are temporally and spatially overlapped and a resonance condition is fulfilled, a small 'slice' of the electron bunch will be modulated in energy and can be split off from the main bunch in a subsequent dipole magnet [22, 23]. The energy-modulated bunch is of the length of the fs laser pulse, i.e. on the order of 50–100 fs and will radiate correspondingly short fs x-ray pulses in a second undulator [23].

This way of generating fs x-ray pulses comes at the cost of a several order of magnitude reduction in x-ray flux [23], as a) only a small slice of the ps electron bunch radiates x-rays and b) the repetition rate is limited to that of the amplified fs laser system used for energy modulation, typically several kHz compared to the e.g. 800 MHz bunch repetition rate at the BESSY II synchrotron. While there is a high sensitivity to pump-induced changes, since Femtoslicing sources are quite stable sources with low shot-to-shot fluctuation, the nevertheless long data acquisition times of several hours per transient spectrum limit the number of parameter sets (e.g. pump fluence, sample thickness or other material changes) that can be investigated during a typical beamtime of 6–12 12 h shifts, which makes systematic parameter variations challenging.

When it comes to the time resolution of pump-probe experiments using x-ray pulses generated by Femtoslicing as a probe, the intrinsic synchronization of pump and probe free of temporal jitter (since both are seeded by the same laser oscillator) is a strong advantage. The x-ray pulse duration is however somewhat limited to that of an amplified laser system with mJ pulse energies, which is required to drive the fs x-ray generation, namely typically 40–50 fs plus pulse stretching by propagation effects in the storage ring as well as due to the monochromator grating [23]. For example, the BESSY II Femtoslicing source achieves an x-ray pulse duration of about 80–100 fs at the sample position, which results in a stable time resolution of 120–150 fs when employing a 40–50 fs short pump pulse.

The beamline and experimental setup (endstation) is designed to mitigate the drawback of very low x-ray flux. At the FemtoSpeX instrument [23] at the UE56/1-ZPM beamline of the BESSY II synchrotron and electron storage ring in Berlin, Germany, which was employed for the experimental work that will be described in section 4.1, this is achieved by employing a single x-ray optical element for focusing and monochromatization: The zone plate monochromator (ZPM) consists of a reflection zone plate designed for maximum x-ray transmission of the beamline. In order to avoid temporal broadening of the fs x-ray pulse, the number of illuminated grating lines/mm is restricted and thereby the energy resolution is limited to $E/\Delta E = 500$ [23]. As the ZPM is the only optical element in the beamline and the Femtoslicing technique lowers the photon flux by several orders of magnitude, no intensity reference for normalization can be acquired, which makes spectral analysis in tr-XAS challenging. However due to alternating pump on/pump off measurements the experiment is very sensitive to pump-induced changes on the order of 10^{-3} [24], together with the generally high stability of the source. This made it possible to achieve a number of groundbreaking results with the BESSY II Femtoslicing source, for example the first tr-XAS and tr-XMCD experiments on ultrafast demagnetization of Ni [25], separation of spin and orbital moment dynamics [26, 27], observation of superdiffusive spin currents driving fs

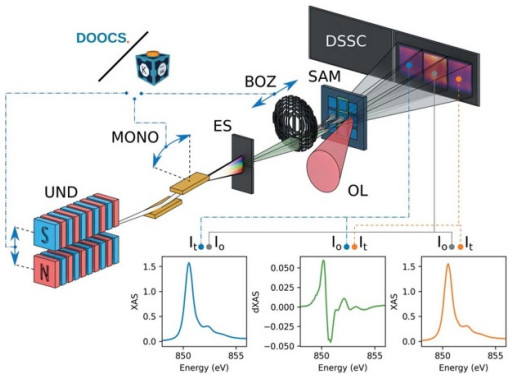

Figure 2. Schematic view of beam-splitting off-axis zone plate (BOZ) setup at the SCS instrument of European XFEL. The x-ray beam from the undulator (UND), which is monochromatized (monochromator, MONO; exit slit; ES) and split into three copies by the BOZ, is transmitted through three windows of the sample (SAM), one of them overlapped with the optical laser (OL), and then imaged on the DSSC detector. Thereby, intensity-normalized (I_0) spectra with and without optical excitation are acquired. Reproduced from [31]. CC BY 4.0.

demagnetization [28], and resolving the sublattice dynamics in all-optical magnetization switching [29]. In section 4.1, I will review the acquisition of time-dependent spectral information in tr-XAS with this Femtoslicing source for the element-sensitive analysis of energy transfer dynamics in heterostructures [24, 30].

2.3.2. XFELs

XFEL sources are based on linear accelerators. While GeV electrons travel through long undulators, see figure 1(b), they interact with the radiation they themselves generate, which leads to sub-structuring of the electron bunches, the so-called microbunching [32]. The microbunched electrons radiate in phase, which leads to amplification of the x-ray intensity (until the process saturates), termed self-amplified spontaneous emission (SASE) [32]. Thereby, FELs have succeeded in generating extremely brilliant fs x-ray pulses.

While FELs produce very short x-ray pulses down to the few fs or even attosecond range, the time resolution in laser pump, XAS probe experiments is however determined by the accuracy of the pump-probe synchronization, which is limited by temporal jitter due to fluctuating arrival times of the x-ray pulses. It can be further improved by measuring this arrival time for each x-ray shot and correcting the pump-probe data accordingly [33, 34]. The time resolution achieved in the FEL work [31, 35–38] discussed in section 4 was 80 fs, limited by temporal jitter within x-ray pulse trains arriving at 10 Hz repetition rate.

Since the x-ray generation in FELs originates from SASE as introduced above, a process which starts from random fluctuations, the x-ray pulses exhibit strong shot to shot fluctuations. This requires a scheme to normalize XAS signals to a pulse intensity monitor, which can for example be a signal from a transmission gas monitor. A new instrumental development is to employ a normalization mechanism with x-ray optics [39] in order to achieve high signal-to-noise ratios despite these fluctuations. [31] shows how such a scheme was implemented at the spectroscopy and coherent scattering (SCS) instrument of the European XFEL in Schenefeld, Germany.

The XFEL radiation coming from the undulator is monochromatized by a variable line space grating monochromator, followed by the exit slit, see figure 2. The monochromatic but unfocused x-ray beam impinges on the beam-splitting off-axis zone plate (BOZ), which splits it into three copies with the same x-ray intensity. These three beams are now transmitted through three separate regions of the sample. Two of them, namely the outer beams in figure 2, travel through two equivalent regions of the sample prepared by large area deposition, e.g. sputter deposition or molecular beam epitaxy (MBE). One of these regions is overlapped with the pump beam from the optical laser, such that the transmitted beams imaged on the large area DSSC detector [40] correspond to XAS in the optically excited respectively ground state. Subtracting one from the other directly produces the pump-induced change, see figure 2. The middle beam is transmitted through a region of the sample array that was masked during sample deposition, so that only the transmitted x-ray intensity of the subtrate (and potential auxiliary layers such as a heat sink) is measured, which provides the reference for normalization of the ground state and pumped spectra to the incoming x-ray intensity. Through this beam-splitting x-ray optics, which provide a referencing scheme for each x-ray pulse, shot-noise limited femtosecond time-resolved XAS is made

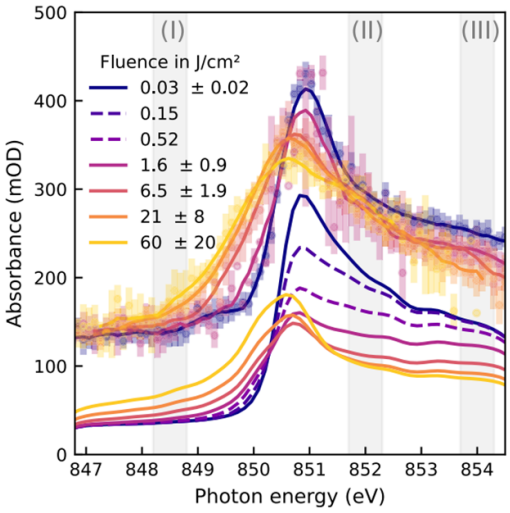

Figure 3. Ni L_3 edge XAS for increasing x-ray fluence as indicated (top curves). Error bars represent 95% confidence intervals and lines smoothed data. Corresponding simulations of the absorption (bottom curves). The two sets of curves are vertically offset with respect to each other for clearer display. Reproduced from [41]. The Author(s). CC BY 4.0.

possible at European XFEL [31]. This is combined with the high repetition rate enabled by superconducting linear accelerators, which further improves the number of detected photons. Herein, the DSSC detector allows to detect the transmitted x-ray intensity through the sample from every pulse and normalize it with the BOZ scheme.

While high repetition rates in the few kHz to 100 kHz range increase the number of detected x-ray photons and thus in principle improve the data quality and ability to measure small transient signals, they come with a drawback. In case the optical laser (pump pulse) impinges on the sample at the same repetition rate, the time between subsequent laser pulses in the stroboscopic experiment might not be long enough for the pump-induced changes to relax entirely. The material under investigation thus does not recover its ground state before the next pump excitation, and long-living states, such as thermal lattice excitation or polaron formation, build up over the course of the measurement. Such long-living process complicate the extraction of actual fs transient events and/or change the state of the sample such that different physical processes occur or it is in a different phase, e.g. an elevated lattice temperature due to permanent heating. These effects are particularly pronounced for thin films on x-ray transparent freestanding substrates such as Si_3N_4 membranes, which are commonly used for XAS in transmission geometry. The reason for this is the poor thermal conductivity across the interface to the membrane as well as its typical thickness of 50–200 nm only. [38] shows that long-living effects, which persist beyond the repetition rate of stroboscopic XAS experiments, can be identified and characterized through careful data analysis procedures and modeling.

The above described setup has been used for the work reviewed in sections 4.2 and 4.3. Moreover, it allows for the investigation of more dilute systems: [36] analyzes thin solid films of spin crossover complexes through time-resolved XAS resonant at the Fe L_3 edge of the central Fe ion of the complex and thereby reveals an intermediate state in the optically induced low to high spin transition on femtosecond timescales in this dilute molecular system.

2.4. Non-linear XAS

At very high x-ray intensities, non-linear effects beyond one-photon (linear) absorption of x-rays start to occur [42]. XFELs provide such high peak intensities with $> 10^{10}$ photons per pulse combined with fs pulse duration. One should firstly make sure not to induce non-linear effects or even sample damage in linear XAS when XFEL pulses are used as a probe in fs pump-probe experiments. This partly motivates an x-ray fluence dependent analysis of XAS. Going beyond these practical considerations, non-linear effects [42] similar to those established in the visible and infrared range can be exploited to gain physical information.

Modifications of the XAS fine structure linked to electronic and spin excitations have indeed been observed in the soft x-ray absorption of metallic thin films at very high x-ray fluences [43]. Engel *et al* [41] provides a further example for such effects. Figure 3 displays L_3 edge absorption spectra of a thin Ni film taken at the SCS instrument of European XFEL with a variation of the BOZ scheme introduced in section 2.3.2, however employing only two x-ray beams measuring the sample absorption respectively

an intensity reference for normalization of the former signal. Through focusing the x-ray beams with the BOZ, see figure 2, it is possible to reach extreme fluences up to 60 ± 20 mJ cm^{-2}. The x-ray fluence is adjusted by translating the sample along the x-ray propagation direction, thus moving into or away from the focal spot, which is on the order of μm.

Figure 3 shows XAS measured with x-ray pulses of 30 fs full width at half maximum duration [41]. When the x-ray fluence is increased, clear fluence-dependent changes to the spectrum are visible. These changes consist of a broadening in the pre-edge region and an intensity decrease and shift of the main absorption feature, see figure 3. With the help of rate model simulations of the x-ray induced electron excitation and subsequent scattering [41], these features can be understood as an effect of increased valence occupation with increasing x-ray fluence, which saturates the Ni L_3 edge resonant absorption, in conjunction with the excitation of valence holes and attendant shift of the chemical potential during the interaction of the x-ray pulse with the material.

3. Non-equilibrium XAS of solids: state of the art

Transient XAS with femto- or picosecond time resolution at synchrotron and free electron laser facilities has been developed over the previous three decades, in parallel to optical, photoelectron or other pump-probe spectroscopy methods, in order to analyze electronic, spin and lattice excitations in solid materials. The following sections will briefly review these experimental achievements. While similar developments have occurred in the non-equilibrium XAS of materials in the gas or liquid phase, this area of research is not a topic of interest for this Topical Review; the reader is referred to corresponding reviews [44–47].

3.1. Probing electronic excitations

XAS in general probes the unoccupied electronic structure of solids. This suggests that transient changes to the electronic occupation driven by optical excitation in pump-probe experiments, e.g. a redistribution of electrons and holes, are reflected in the time-dependent x-ray absorption spectrum as well. Moreover, the electronic states, or band structure, of a solid might itself undergo changes in the non-equilibrium state after pump excitation, which can be expected to alter the x-ray absorption spectrum too. Such effects have previously been investigated in metals, semiconductors and strongly correlated oxides. Information on the non-equilibrium dynamics is derived from transient spectral signatures in XAS, and the time-dependence of these features.

Figure 4 depicts different excitation processes and the resulting transient modification of a generic transition metal L_3 edge x-ray absorption spectrum schematically. Electronic structure changes like an energetic shift of the $3d$ states likewise lead to a shift in the x-ray absorption spectrum. In a simple picture, optically induced changes in the electronic occupation can generally manifest in two ways: An initially non-thermalized hole population opens new channels for transitions from the core level into unoccupied states, which manifests as additional absorption features, as depicted for a pre-edge feature in figure 4. Such an energetically localized transient signature is more likely for a semiconducting or insulating solid, as in metals electron and hole scattering times are on the order of fs, thus leading to a rapid thermalization of electron and hole population. In metals, a thermalized electronic population follows a Fermi distribution, which is energetically broadened at elevated electronic temperatures. The attendant redistribution of unoccupied states then leads to increased absorption at photon energies below the absorption edge, respectively decreased absorption at or above the edge, compare figure 4.

In the transition metal ferromagnet Ni, a transient shift of the L_3 edge x-ray absorption spectrum to lower photon energies was indeed observed after optical excitation [25]. Along with subsequent experiments on the same material [48], which confirmed the transient redshift and found that it scaled linearly with pump fluence, i.e. excitation density, these observations were linked to the generation of hot electrons after laser pumping, accompanied by changes to the valence electronic structure, compare figure 4. Specifically, the spectral changes were reproduced by cluster calculations assuming a reduced $3d-4sp$ hybridization, which was assumed to be caused by the presence of hot electrons on fs [25] respectively phonon excitations involving spin-flip processes on ps timescales [48].

Interestingly, qualitatively similar observations of transient shifts of core level absorption edges coupled with increased absorption in the pre-edge region were made in rather different excitation regimes, namely upon plasmon excitation of Au nanoparticles [49] and in the warm dense matter state of Cu [50–52]. In the former case, the absorption increase was correlated to the presence of hot holes, and correspondingly the absorption reduction to the filling of previously unoccupied states by hot electrons, after non-radiative decay of the plasmon [49]. In the warm dense matter regime, the elevated electronic temperature could be determined from the time-dependent spectral shift and broadening on

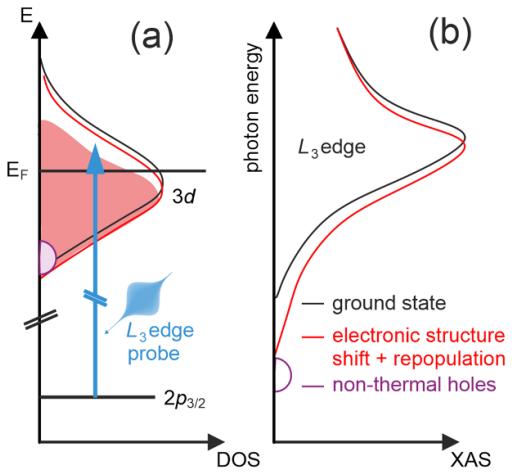

Figure 4. (a) Schematic depiction of transition metal 3*d* density of states and x-ray L_3 edge probe transition starting from the $2p_{3/2}$ core level. Pump-induced changes in the electronic population are visualized with red shading, while changes in the electronic structure itself are shown by the red line. The presence of non-thermalized holes is indicated in purple. Note that these pump-induced changes are depicted in an exaggerated manner for better visualization. (b) Schematic ground state XAS at the L_3 edge (black), transient shift and broadening due to electronic excitation (red) respectively additional absorption due non-thermal holes (purple).

few ps timescales [50], while the 3*d* band shifts on sub-ps timescales [52]. The observation of increased pre-edge absorption and energy shifts in resonant tr-XAS of metals thus appears to be a general feature linked to the generation and redistribution of electronic population at elevated electronic temperatures.

In the rare earth ferromagnet Tb, transient changes at the M_5 edge were found to originate from 4*f* multiplet excitations caused by inelastic scattering of 4*f* and 5*d* electrons [53]. A subsequent analysis of the $M_{5,4}$ branching ratio found that these excitations alter the total angular momentum *J* in the non-equilibrium state after optical excitation [54]. These observations link to the probing of spin excitations with tr-XAS, which will be further discussed in section 3.2.

In semiconducting Ge thin films, the photo-generation of non-equilibrium electrons and holes accompanied by band shifts was probed simultaneously at the $M_{5,4}$ edge through spectral shifts and broadening [55]. Coming to layered materials, time-resolved XAS at the carbon *K* edge of semi-metallic graphite showed, through a mapping between the absorption spectrum and the unoccupied DOS, asymmetric dynamics above compared to below the Fermi level [56]. The thus extracted electron and hole relaxation times revealed strongly enhanced charge carrier lifetimes in the region of flat bands due to the suppression of carrier-carrier scattering [56]. Common features among these experimental findings can be related to the above discussed transient redshift in transition metals, as both observations results from pump-induced changes to the electronic occupation. The sensitivity of XAS to electrons and holes in metals and semiconductors thus appears to be similar, while noting that in semiconductors these are two separate charge carrier populations, i.e. electron and hole populations in the conduction respectively valence bands, in contrast to metals. In the latter material class, transient XAS reflects transient redistribution of population throughout the whole vicinity of the Fermi level.

The creation of holes in the valence band of a photo-excited lead halide perovskite was found to induce transient Br *K* pre-edge features [57]. Considering the timescale of $\geqslant 100$ ps, it is likely that these charge carriers are already trapped by polaron formation, which typically takes place on few ps or even sub-ps timescales [58, 59]. Polaron formation was indeed found to be the origin of other transient features in the same experiment [57], as will be discussed in section 3.3.

Hot charge carrier relaxation in Co_3O_4 has been monitored at the Co $M_{2,3}$ edges [60]. In Fe_2O_3, a transient oxidation state change after optically driven ligand-to-metal charge transfer was identified in Fe $M_{2,3}$ edge tr-XAS [61], followed by the relaxation of the charge transfer excitation and transition into a polaron state [59, 61]. These findings were confirmed by Fe L_3 edge tr-XAS [62], while the decay of the valence hole within 200 fs was tracked by O *K* edge tr-XAS [63]. Trapping of photo-generated holes in TiO_2 was analyzed via Ti $L_{2,3}$ and O *K* edge tr-XAS [64]. The tr-XAS technique was also applied to the investigation of charge carrier dynamics following optically induced ligand-to-metal charge transfer in $CuWO_4$ [65] and $LaFeO_3$ [66]. The observation of charge carriers trapped by polaron formation, i.e. combined electronic-structural excitations, through tr-XAS, connects to the sensitivity of tr-XAS to phonons, which is treated in more detail in section 3.3. It should be noted that different points of

view toward such a combined electronic-structural excitation are found in the literature, depending if the interpretation of the respective transient spectra is more closely linked to electronic versus structural changes.

In transient x-ray linear dichroism spectroscopy at the Zn *K* edge of ZnO nanorods, a separation of non-thermal from thermal contributions was performed by means of a comparison with temperature-dependent EXAFS spectra, thus revealing the presence of free electrons in the ZnO conduction band [67]. This work demonstrates that a suite of x-ray spectroscopic techniques can work together to isolate specific charge carrier populations, as the transient EXAFS measurements also ruled out structural distortions associated with trapped carriers [67]. Follow-up time-resolved XAS experiments at the Zn *K* and L_3 edges of ZnO thin films showed that transient blueshifts at the core level excitonic resonances are tunable through the excitation density, indicating that they are sensitive to excited free carriers via changes in the Coulomb screening [68].

The analysis of electronic excitations through tr-XAS has also been applied to two-dimensional materials. Semiclassical theory predicts that attosecond transient XAS is sensitive to photoinduced changes of the Berry connection or curvature in graphene [69, 70] and hexagonal boron nitride [71], possibly enabling the tracking of topological phase transitions [72] as well as valley-selective excitations [73, 74]. Experimentally, electron–hole relaxation [75] as well as inter- and intraband charge carrier dynamics in $MoTe_2$ have been analyzed by tr-XAS [76]. In WS_2, hole relaxation and recombination dynamics was studied [77], while in WSe_2 also a phonon-mediated band shift on the timescale of the hole relaxation was observed [78]. Signatures of charge density wave excitations were found in transient XAS of $TiSe_2$ [79].

Femtosecond tr-XAS has in recent years emerged as a new tool to address dynamical interactions in strongly correlated materials. In the cuprate superconductor $La_{1.905}Ba_{0.095}CuO_2$, the O *K* and Cu L_3 edges both showed a transient redshift of features associated with the upper Hubbard band (UHB) after photo-excitation, from which a renormalization of the on-site Coulomb repulsion at the Cu sites of about 140 meV was concluded, while the energy position of a O *K* edge feature related to the Zhang-Rice singlet stayed constant [80]. In the charge transfer insulator NiO, transient changes in the O *K* tr-XAS that are only present within the 150 fs duration of the pump pulse were assigned to the dynamical Franz–Keldysh effect [81], while spectral modifications that persist beyond this ultrashort timescale were linked to magnon excitation [82]. Recently, the orbital selectivity of resonant soft x-ray scattering was exploited to investigate charge ordering phenomena in an infinite-layer correlated material [83]. Further examples for the manifestation of electronic correlations and transient modifications of electronic screening in tr-XAS will be discussed in detail in sections 4.2 and 4.3.

3.2. Analysis of spin excitations

X-ray absorption methods are generally sensitive to spin excitations in two ways: First, via x-ray magnetic circular or linear dichroism, which probes long-range ferro- or ferrimagnetic order respectively antiferromagnetic order as well as magnetic moments induced by electronic hybridization at interfaces [19, 20], secondly through spectral signatures in XAS that are sensitive to the spin state of a molecule or solid [84]. Correspondingly, time-resolved XMCD and XMLD have been employed for the analysis of pump-induced magnetization dynamics [4, 85], while optically driven changes to the spin state have been investigated with transient XAS [84].

XMCD refers to the difference in the absorption of circularly polarized x-rays for right and left circular polarization direction, or respectively opposite orientation of the magnetization vector for fixed circular polarization direction. It measures the projection of a ferro- or ferrimagnetic sample's magnetic moment on the x-ray propagation direction, for the specific element which is resonantly probed at a core-level resonance. The so-called XMCD sum rules allow to derive spin and orbital moments by measuring XMCD [86]. Consequently, in time-resolved XMCD experiments the data of interest are time-dependent XMCD signals proportional to spin and orbital moments, or the values of these moments which are calculated from sum rule analysis, in combination with the element-specific magnetization dynamics.

Transition metal ferromagnets have been investigated with time-resolved XMCD in a complementary manner to the transient XAS experiments discussed in section 3.1. Pioneering experiments by Stamm *et al* verified the optically induced demagnetization of Ni by tr-XMCD [25]. Subsequent work employing the XMCD sum rules [26, 27] found that spin and orbital angular momentum decreases concurrently during ultrafast demagnetization.

The element-specificity of the core level transitions involved in XMCD have been proven particularly useful for an element-sensitive probing of optically induced demagnetization in ferromagnetic alloys

like NiFe [87] or magnetization switching in ferrimagnetic alloys like GdFeCo [29], as well as the competition between spin transfer and spin flip processes in Heusler alloys [88]. In elemental rare earths and their alloys, the influence of the strength of the 4*f* orbital spin-lattice coupling [89, 90] and of the type of magnetic order [91] on the timescale of optically induced demagnetization were revealed. In ferromagnetic heterostructures, tr-XMCD with femtosecond time resolution made it possible to analyze optically driven spin-dependent charge currents [28, 92] by element-selectively probing different layers into which currents are injected or generated from. Layer-selectivity via tr-XMCD has recently also been employed to characterize magnetization switching by optically driven spin currents [93]. Moreover, the acceleration of magnetization dynamics in ferromagnet/antiferromagnet bilayers [94] as well as heterostructures with antiferromagnetic coupling through spin transfer [95] was investigated through fs tr-XMCD. Recently, an optically induced magnetic moment increase linked to the valence band spin texture in two-dimensional magnetically ordered materials was predicted to be detectable via fs tr-XMCD [96]. It should be further noted that pump-probe XMCD at synchrotrons can also be employed to analyze spin pumping after radio frequency spin wave excitation, for example in ferromagnet-topological insulator-ferromagnet heterostructures [97].

Lastly, optically induced changes to the magnetic order could be revealed through XMCD in transient reflectivity: In ferromagnetic $BaFeO_3$, an ultrafast demagnetization acceleration with increasing excitation density was found and linked to an increased susceptibility of the insulating oxide to demagnetization in the course of a photo-induced insulator-to-metal transition [98]. The observation of a transient ferromagnetic XMCD signal at the L_3 edge of antiferromagnetic Mn in Co/Mn multilayers during optically driven demagnetization of Co, tracked via its L_3 edge tr-XMCD, was explained by spin-dependent charge transfer at the interfaces [99]. The combination of tr-XMCD at the Fe L_3 edge and tr-XMLD at the Co L_2 edge of Fe/CoO bilayers revealed that hot electron transfer at these ferromagnet/antiferromagnet interfaces mediates ultrafast demagnetization [100]. A fuller overview over ultrafast spin dynamics in solids, including their characterization by x-ray techniques, is provided by recent reviews [4, 101–103]. The interaction of spin dynamics with signatures of electronic band structure changes will be discussed for an exemplary case in section 4.2.

Other than x-ray magnetic dichroism in materials with long-range magnetic order, time-resolved XAS has been employed for the analysis of spin-dependent excitations, namely transient spin state changes in spin-crossover materials in the solid phase. The XAS fine structure of the central transition metal ion in this material class typically exhibits a characteristic line shape linked to the spin state. Consequently, these signatures can be employed to track the evolution of the spin state after perturbation by, e.g. a femtosecond optical pulse [84, 104].

In $LaCoO_3$, an optically induced spin state transition was probed through resonant XAS of all constituents of the oxide [105, 106], finding a laser-driven metallization, which stabilizes within 3 ps [106] at the La *M* edges and O *K* pre-edge as well as spin-related spectral changes at the Co *L* and O *K* edges [105]. An optically pumped charge transfer excitation in nickel ferrite was found to result in charge carrier localization due to polaron formation, which in turn induced a transient spin state change within ≈300 fs through modifications of the Ni crystal field splitting [107]. For this and the preceding case, the element- and site-specificity of resonant tr-XAS was crucial to gain insight into the complex evolution of the non-equilibrium state in oxides.

In thin molecular films of spin-crossover complexes, fs tr-XAS enabled the tracking of the crossover from a low to a high spin state through the time-dependence of the absorption change at the respective spectral features of the Fe L_3 edge of the central iron ion, and thus revealed an intermediate state during optically induced spin state switching [36]. Element-sensitive transient XAS with the approx. 70 ps time resolution of the BESSY II synchrotron allowed to distinguish the degree of charge delocalization of different spin states in mixed-valence complexes [108]. For a more extensive discussion of the ultrafast dynamics of spin-crossover complexes probed with x-ray techniques, the reader is referred to recent reviews [84, 104].

3.3. Sensitivity to lattice excitations

While lattice excitations in solids are typically probed with time-resolved x-ray [109–111] or electron diffraction methods [112], time-resolved XAS is also sensitive to them. Such a sensitivity is more established in the EXAFS region [21, 113, 114]. However, near-edge transient fine structure changes can be employed to analyze excitations that involve ion core motion as well, as will be discussed in the following.

Figure 5 gives an overview over possible contributions by schematically showing how a generic oxygen *K* edge x-ray absorption spectrum can be modified by different excitations of the lattice degree of

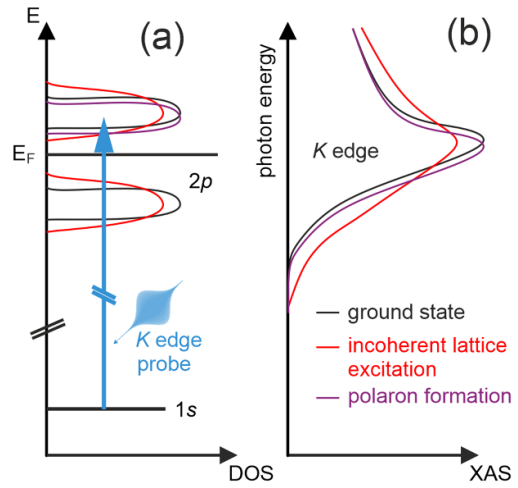

Figure 5. (a) Schematic depiction of oxygen 2*p* density of states of an oxide and x-ray *K* edge probe transition starting from the 1*s* core level. Changes in the electronic structure mediated by incoherent lattice excitation respectively polaron formation are visualized red respectively purple. Note that these transient changes are depicted in an exaggerated manner for better visualization. (b) Schematic ground state XAS at the *K* edge (black) and transient shift due to polarons or other structural modification (purple) respectively broadening due to incoherent lattice excitation (red).

freedom. Incoherent lattice excitation involves an average displacement of the ion cores from their equilibrium positions, which can be understand as disorder that leads to broadening of electronic states, and consequently broadening of the XAS fine structure [30]. Such XAS changes can also be explained by extending the model picture behind EXAFS, i.e. the interaction of the outgoing photoelectron wavefunction with the motion of the neighboring ion cores, into the NEXAFS region [30]. In contrast, the trapping of photoexcited charge carriers involving polaron formation, or other structural changes in which bonds lengths or angles are transiently changed, might renormalize transitions and thus lead to shifts in the x-ray absorption spectrum, compare figure 5.

In practice, it might in fact be difficult to distinguish these contributions, with a comparison to time-resolved diffraction experiments and/or static temperature-dependent XAS being beneficial for assigning spectral signatures. Similar spectral signatures as observed in temperature-dependent experiments suggest thermal lattice excitation, while a comparison of the relaxation times in transient XAS to those found with complementary time-resolved diffraction methods can facilitate an assignment to lattice as opposed to purely electronic excitation. In the lead halide perovskite $CsPbBr_3$, such an approach was indeed applied to distinguish polaron formation from thermal excitation and a thermally induced structural phase transition [57]. By means of a comparison to temperature-dependent spectra, polaron formation at Br centers upon optical excitation was identified via distinct transient lineshape changes of the Br *K* edge [57]. Furthermore, the resulting bond distortion was quantified through a comparison with band structure calculations [57], which highlights the potential of tr-XAS to deliver quantitative information on non-equilibrium states in conjunction with theory. In earlier experiments, the verification of the formation of reduced and structurally distorted sites assigned to small polaron formation in iron oxide nanoparticles had been strongly dependent on a qualitative comparison with simulations of the transient Fe *K* edge spectra [115]. In TiO_2 nanoparticles, a transient redshift of the Ti *K* edge within ≈300 fs was linked to trapping of photo-excited charge carriers, in conjunction with transient changes of pre-edge features, which originate from weakly allowed 1*s*-3*d* transitions that are strongly sensitive to local lattice symmetry [58]. The combination of time-resolved XANES at the Ce L_3 edge with transient EXAFS provided further insights into polaron formation in CeO_2 [116]. Here, the transient XANES changes were explained by a mixture of oxidation state changes and thermal lattice excitation, while an expansion of the Ce-O distance consistent with polaronic distortion was concluded from tr-EXAFS [116].

Polaron formation has been observed with tr-XAS in a wider class of materials and at lower x-ray photon energies than the just discussed hard x-ray tr-XAS results [57, 58, 115, 116]. In Fe_2O_3, a transient redshift of the Fe M_{23} edges in the extreme ultraviolet (XUV) range, which followed an optically induced charge transfer excitation (compare section 3.1), was linked to small polaron formation [59]. The simultaneous sensitivity to tr-XAS to electronic excitation and structural distortion made it possible to track the sequence of excitations by the timescale of the decay of spectral features associated with the charge transfer state respectively appearance of the polaron state features. Similar observations in the

transient Ni M_{23} edge XAS of NiO likewise were assigned to small polaron formation [117]. This and other recent developments in tr-XAS, increasingly employing laboratory-based x-ray sources, highlight the ability of tr-XAS to probe coupled electronic and structural dynamics [118].

Angle-dependent resonant x-ray reflectivity has been employed to perform depth profiling of ferromagnetic films and therefore conclude on the generation of transient strain or lattice expansion during optically induced magnetization dynamics [119, 120]. Exploiting magnetic circular dichroism at core level resonances allowed to simultaneously probe the depth dependence of the pump-induced magnetization changes [119]. Transient changes in the magnetization-independent reflectivity at the Ni L_3 edge indicated that ultrafast demagnetization of a thin Ni film is accompanied by a transient strain wave involving a lattice compression of up to 1% perpendicular to the sample surface within ≈200 fs, followed by expansion of a similar magnitude on few ps timescales [119]. Similar experiments at the Fe L_3 edge of a thin Fe film revealed an inhomogeneous sub-ps demagnetization along the depth of the film as well as a subsequent thickness oscillation driven by a coherent strain wave [120].

Together, these results demonstrate that tr-XAS is sensitive to incoherent lattice excitation, polaron formation and transient strain, i.e. coherent acoustic waves. The simultaneous tracking of electronic structure and/or spin dynamics with tr-XAS, i.e. under the exact same experimental conditions, is a strong benefit of the technique, since it avoids experimental uncertainties arising from the comparison of measurements performed at different facilities or laboratories with potentially varying excitation conditions or sample properties. An exemplary analysis of incoherent lattice excitation with time-resolved XAS will be discussed in the next section 4.1.

4. Exemplary insights from time-resolved XAS

4.1. Non-equilibrium energy transfer dynamics in metal/insulator heterostructures

4.1.1. Motivation

Solid heterostructures, consisting of two or more thin films or atomically thin layers of different materials, are the basic building blocks of many applications in (opto-)electronics and spintronics. Their functionality depends on charge and energy transfer processes between their components, i.e. across the interface(s) of the heterostructure. While the understanding of fundamental processes, namely electron–electron and electron–phonon scattering leading to charge carrier thermalization and energy transfer to the ion cores, has been advanced significantly through pump-probe experiments, simulations and ab initio theory over the last decades, as introduced in section 1, open questions remain when going from bulk materials to heterostructures: On which timescale and via which processes is energy transferred across the interface? Is the transfer mediated by electrons, phonons, or both? The latter is particularly relevant if one or more layers of the heterostructure are insulating or semiconducting, as the injection of charge carriers across the interface can be inhibited depending on the matching, or hybridization, of the electronic structure of the constituents. The interface properties are also likely to play a role, through electronic and vibrational hybridization as well as the interface morphology, e.g. roughness or interdiffusion, which affect scattering processes.

These questions touch on the problem if assuming thermalized distributions, as for example done in the commonly used 2TM [10], is valid on femto- to picosecond timescales after optical excitation. The presence of multiple components means that more scattering channels across heterostructure interfaces are open compared to bulk. Scattering and transfer processes within the layers and between them might also compete, further complicating the view. With respect to the lattice degree of freedom, it was moreover recently found that non-equilibrium in the phonon system can persist for a comparatively long time, as anharmonic processes leading to phonon-phonon scattering and thermalization take tens of ps [12].

In the following, I will review how the element-sensitivity of tr-XAS can disentangle the optically induced dynamics in different components of a metal/insulator heterostructure, including energy transfer processes across the interface between them [24, 30]. Crucially, both the spectral shape of the transient XAS features and their time dependence provides information on the nature of these processes.

4.1.2. Results and discussion

The investigated model metal/insulator heterostructure consists of 8 repetitions of a Fe/MgO double layer with Fe and MgO thicknesses of 2 nm each. The samples were prepared by MBE as polycrystalline layer stacks on Si_3N_4 substrates for transmission XAS measurements (see section 2.2). Notably, the interface characterization by Mössbauer spectroscopy showed that intermixing between Fe and MgO

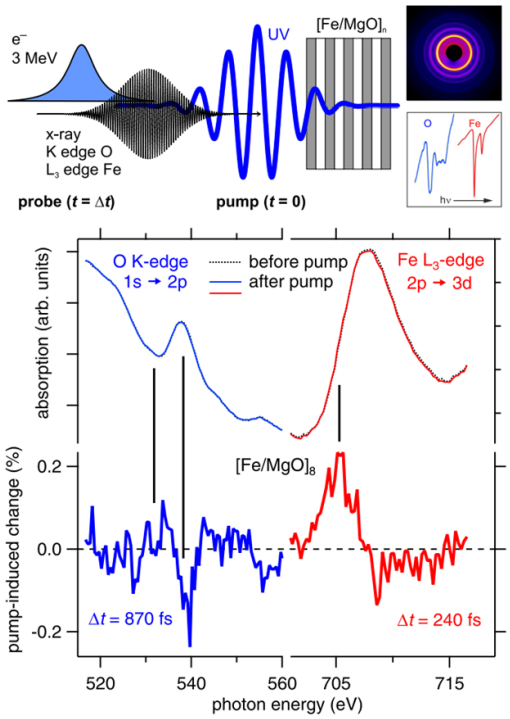

Figure 6. (top) Experimental scheme of UV pump, tr-XAS respectively ultrafast electron diffraction (UED) probe experiment with exemplary UED respectively XAS data shown on the very right. In both experiments, the probe beams are transmitted through the Fe/MgO heterostructure sample. (bottom) XAS before (dashed) and after UV pump (solid lines) at the O *K* (blue) and Fe L_3 (red) absorption edges, with the pump-induced change at the indicated pump-probe delays Δt. Reprinted (figure) with permission from [24], Copyright (2019) by the American Physical Society.

at the interfaces is limited to a monolayer thin region only [24]. Therefore, a possible influence of interface morphology and roughness on the dynamics discussed in the following can be minimized. Further details on the sample preparation and characterization are given in [24].

In order to track the energy flow in the Fe/MgO heterostructure, the pump photon energy is chosen in the UV range, namely 4.7 eV [24]. With this photon energy, hot electrons are excited that are energetic enough to in principle cross the charge transfer gap of 3.8 eV from the Fe Fermi level to the MgO conduction band [121]. This photon energy is much less than the MgO band gap, such that, together with the still moderately high incident pump fluence of ≈20 mJ cm^{-2}, MgO is not directly excited by either one- or two-photon-absorption [24]. The initial excitation is therefore localized in the Fe layers of the heterostructure.

The element-sensitivity of tr-XAS at the BESSY II Femtoslicing facility (see section 2.3.1) is then exploited to separate the optically induced dynamics in the Fe respectively MgO layers via resonantly probing the Fe L_3 respectively O *K* edges in transmission geometry, see figure 6. The O *K* edge shows an intensity reduction or broadening of the absorption peak, while the derivative-like transient signature at the Fe L_3 edge hints at a redshift, i.e. a shift of the absorption edge to lower photon energies. An initial interpretation of the pump-induced changes can be made via the timescales of excitation and relaxation. First of all, the timescales of the pump-induced changes are clearly different at the Fe L_3 compared to the O *K* edge, see figure 7, with the maximum change at the Fe L_3 edge being reached at about 200 fs after optical excitation, while the transient change at the O *K* main absorption peak still builds up at that delay and finally saturates at around 1 ps. Keeping the energy level alignment in the Fe/MgO heterostructure introduced above in mind, it is consequently the case that the excitation of the MgO layers does not occur via injection of hot electrons, as the transient change at the O *K* main absorption peak only becomes prominent when that at the Fe L_3 edge already relaxes, due to thermalization of hot electrons and electron–phonon scattering (compare figure 7). The hot electrons with an initial excess energy of up to 4.7 eV are thus unable to cross the charge transfer gap before relaxing towards the Fe Fermi level. For strengthening the assignment of the underlying processes based on their timescales, a comparison with complementary ultrafast electron diffraction (UED) is highly beneficial. UED probes the mean-square atomic displacement, i.e. incoherent lattice excitation, of the Fe layers at the diffraction peak chosen here [24]. The direct comparison of tr-XAS and UED in figure 7 confirms that the excitation of MgO, as probed by the O *K* main absorption peak, proceeds on the same timescale as incoherent

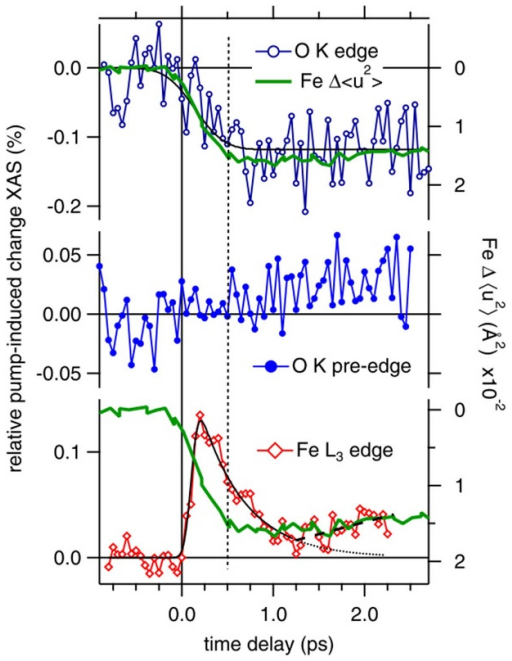

Figure 7. Pump-induced change in XAS at the O *K* edge main peak (top) and pre-edge feature (middle) as well as the Fe L_3 edge (bottom). Mean-square atomic displacements of Fe from UED are shown as green solids lines in comparison. Reprinted (figure) with permission from [24], Copyright (2019) by the American Physical Society.

lattice excitation of Fe. With ab initio calculations of the vibrational DOS at the Fe/MgO interface [24], these lattice excitations can be assigned to hybrid interface phonon modes that provide an additional channel for hot electrons in Fe to couple to and thus transfer energy not just to phonon modes in the bulk of Fe but also across the interface into MgO.

This finding shows that a) dynamics in different constituents of a heterostructure can indeed be tracked through the element-sensitivity of tr-XAS and b) reasonable inferences on the underlying process can be drawn from the timescales alone. Moreover, the transient XAS signatures themselves provide further information. This becomes evident with a deeper analysis of the transient change at the O *K* edge. Employing the native x-ray pulse duration of ≈70 ps of the BESSY II synchrotron enables a more systematic analysis of the O *K* edge fine structure changes at 90 ps [30], when the whole heterostructure can safely be considered thermalized at a common, elevated lattice temperature. The O *K* edge fine structure exhibits an intensity decrease of the absorption peak and filling in of the valleys, i.e. an overall broadening of the near-edge features [30]. This broadening increases linearly with increasing pump fluence, which corresponds to an increasing lattice temperature after equilibration, compare the inset of figure 8. By means of DFT using the alloy analogy model [30], the O *K* edge spectra are calculated and shown in figure 8 in comparison with the experimental pump-induced change at 90 ps delay. Through the good correspondence of experiment and theory, transient broadening as a spectral signature can be linked to lattice excitation and calibrated with an absolute temperature increase (with respect to the initial temperature of 300 K) with the help of theory. Crucially, this finding demonstrates the sensitivity of transient XAS to lattice excitations also in the near-edge region, not only the EXAFS region, where sensitivity to lattice motion is more established [21, 113, 114]. A comparison of the above discussed O *K* edge tr-XAS at 90 ps (figure 8) to the sub-ps dynamics shown in figure 6 indicates through a similar spectral broadening that the transient change indeed originates from lattice excitation, namely the interface phonon modes which extend into MgO and are excited by hot electrons in Fe.

As a last aspect of the MgO tr-XAS, it is notable that the O *K* pre-edge feature exhibits a markedly slower dynamics than the main absorption peak, see figure 7. A further comparison with the timescale of thermalization of the whole heterostructure derived from UED [24] as well as the slower dynamics at the Fe L_3 edge starting from ≈1 ps (see figure 7) indicates that this transient change stems from the thermalization of the whole heterostructure, i.e. the equilibration of the lattice temperature between the Fe and MgO layers. The O *K* pre-edge feature originates from hybridized electronic states at the Fe/MgO interface, while are particularly sensitive to lattice expansion due to their energetic position close to the Fe Fermi level [24]. This observation thus shows the potential to use more detailed spectroscopic information for interface-sensitivity, even though XAS in transmission geometry as used here is

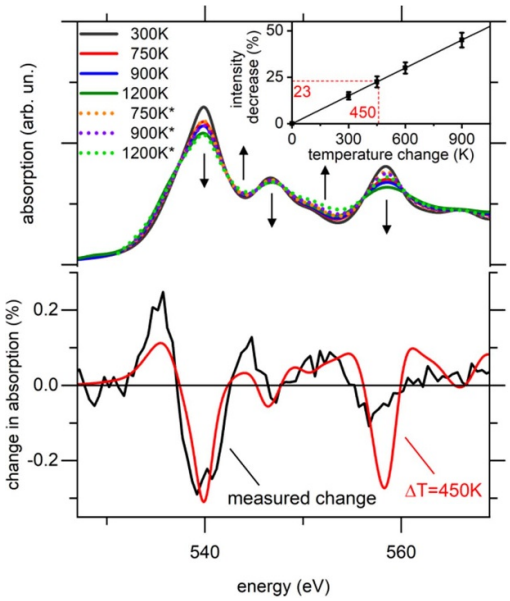

Figure 8. (top) O *K* edge spectra for the indicated lattice temperatures calculated by DFT using the alloy analogy model (solid), together with a modeled intensity decrease of the XAS fine structure based on the 300 K spectrum (dotted lines). The inset shows the linear relation between XAS intensity decrease and temperature change. (bottom) Experimental (black) and calculated (red line) change in XAS for a lattice temperature increase of 450 K. Reprinted (figure) with permission from [30], Copyright (2021) by the American Physical Society.

in principle a bulk probe. Moreover, it demonstrates that energy transfer occurs on different timescales involving different phonon modes, which implies that the phonon system is not in thermal equilibrium on sub-ps timescales when high energy, hybrid interface phonons mediate energy transfer from Fe to MgO. From several ps onwards, lower energy phonons then mediate the thermal equilibration of the whole heterostructure.

In addition, the presence of the interfaces to MgO also influences the magnetization dynamics of the Fe layers after optical excitation: Monitoring the ultrafast demagnetization at the Fe L_3 edge with fs time-resolved XMCD reveals an increasing magnitude of the magnetization decrease with decreasing Fe thickness (at otherwise constant excitation conditions and sample properties) [122]. This effect is linked to a local weakening of the spin order at the Fe/MgO interfaces, which becomes increasingly significant for Fe layers thinner than 10 nm, compared to the bulk-like properties of thicker layers [122].

The transient redshift at the Fe L_3 edge (figure 7) can, since XAS probes the unoccupied electronic DOS, intuitively be linked to excitation of hot electrons: The absorption of the pump pulse shifts electronic population into previously unoccupied states, while holes are generated below the Fermi level, thus transiently changing the final states available for the L_3 edge transitions (compare figure 4). However, the limited energy resolution in these experiments performed at the BESSY II Femtoslicing source (see also section 2.3.1) obscures the full spectral information. Transient spectral shifts will thus be addressed in greater detail with the help of XFEL tr-XAS experiments in the following sections, for a transition metal ferromagnet in section 4.2 and for an oxide in section 4.3.

In the work reviewed in this section, tr-XAS has been employed to analyze ultrafast dynamics at the interface of a solid heterostructure that has been extensively studied over the last decades. More recently, dynamic processes at interfaces between layered materials, such as transition metal dichalcogenide heterobilayers, have come into focus due to the versatility of this material class and the possibility to tune electronic excitations, in particular interlayer excitons [123], and even exploit twist angles to generate Moiré superlattices [124]. Transient XAS is likely to contribute to the analysis of charge and energy transfer processes in such heterobilayers in the future, especially since it was already applied to single layers [76–79].

4.2. Ultrafast charge and spin dynamics in metallic ferromagnets

4.2.1. Motivation

Electron dynamics in the transition metal ferromagnets Fe, Ni and Co have been studied extensively with various pump-probe methods. It is now well established that, after optical excitation, the initially non-equilibrium electron distribution first thermalizes via electron–electron scattering and then the

excess energy is transferred to the lattice through electron–phonon coupling. The non-equilibrium in the electronic system is accompanied by a transient, sub-ps reduction of the magnetization termed ultrafast demagnetization [6, 11]. Due to the exchange-split band structure, electronic lifetimes become spin dependent [1]. This leads to spin-dependent charge transport out of the ferromagnetic layer or probed sample volume [4, 125], which consequently constitutes one contribution to ultrafast demagnetization. In addition, spin-flip scattering processes mediated by spin–orbit coupling [8] and electron–phonon scattering [126] take place. These processes go hand in hand with a transient redistribution of the electron population during transport and scattering. In addition, electronic structure changes occur under non-equilibrium conditions [127]. While the influence of electronic correlations on the ground state properties of transition metal ferromagnets is well known, their possible role on fs timescales has mostly been neglected, with the exception of a recent discussion of memory effects in ultrafast demagnetization [128].

In this context, fs tr-XMCD was first exploited to verify and quantize ultrafast demagnetization, in response to work criticizing time-resolved magneto-optical measurements due to a possible influence of optical artifacts, i.e. signals of non-magnetic origin [129, 130]. In conjunction with tr-XMCD, tr-XAS of Ni [25, 27] and CoPd alloy [26] were measured. These experiments were performed at the BESSY II Femtoslicing source (see section 2.3.1). They demonstrated that the optically driven reduction of the atomic magnetic moment is genuine [25] (for both spin and orbital contributions [26, 27]) through tr-XMCD, while tr-XAS revealed a transient redshift of the transition metal L_{23} edges [25, 27] as observed for the Fe/MgO experiments discussed in section 4.1. However, as could be seen for these Fe/MgO experiments, Femtoslicing sources are so far limited in the achievable energy resolution and data quality. This motivates a closer look at transient XAS signatures in transition metal ferromagnets.

Exploiting the strongly improved signal-to-noise ratio as well as time and energy resolution in tr-XAS experiments at European XFEL through the use of the newly implemented instrumentation [31] described in section 2.3.2, detailed insight into transient XAS features becomes possible, which allows for a direct comparison with ab initio theory and thereby the discovery of the influence of electronic correlations [35].

4.2.2. Results and discussion

Polycrystalline Ni films of 20 nm thickness were prepared by MBE on Si_3N_4 substrates for transmission XAS measurements (see section 2.2). More details of the sample preparation and characterization are provided in [35]. A pump photon energy of 1.5 eV, incident pump fluence of $\approx$12 mJ cm^{-2} and pulse duration of 35 fs was chosen, as these are typical optical parameters for driving hot carrier excitation close to the Fermi level and the attendant ultrafast demagnetization in transition metal ferromagnets.

These optically induced dynamics are probed at the Ni L_{23} edges, see figure 9. The corresponding 2*p* to 3*d* transition probes the 3*d* orbitals in the final state, i.e. the orbitals that carry the major part of the Ni magnetic moment and whose local correlations are of interest here as discussed above. Employing the instrumentation at the SCS instrument of European XFEL described in section 2.3.2, it is now possible to analyze the full spectral information on femtosecond timescales, as it provides fs tr-XAS with significantly improved energy- and time resolution compared to earlier Femtoslicing experiments reviewed in section 4.1.

After optical excitation, the Ni L_3 edge exhibits a derivative-like transient change, see figure 9, which at first glance appears similar to that observed at the Fe L_3 edge of Fe/MgO heterostructures [24] (compare figure 6). However, due to the improved energy resolution and increased signal-to-noise ratio, it is now possible to identify that this transient change is caused by both a redshift and a broadening of the absorption edge. These two contributions can be extracted and separated through model fits (see figure 9), which are described in detail in [35, 38]. This hints at two different processes behind the observed dynamics.

The time dependence of the transient change is shown in figure 10. It reaches a maximum within the first 400 fs and subsequently relaxes in two steps, with about half of the pump-induced tr-XAS change receding within approximately 1 ps, and a long-living residual change, which is most likely due to the slow heat transport out of the excited film (compare section 2.3.2). A comparison with different ab initio calculations is made according to the respective time range: At longer times of > 0.5 ps, density function theory (DFT) with a hot electron distribution, i.e. elevated electronic temperature, and a reduced atomic magnetic moment that accounts for the optically induced demagnetization [35], describes both the spectral features and temporal evolution of tr-XAS, see 10.

On timescales < 0.5 ps, a direct comparison of the transient XAS features and TDDFT clarifies the nature of the initial electron dynamics before thermalization. Considering only the electronic repopulation, which includes spin-flip scattering from the majority to minority spin channel mediated by

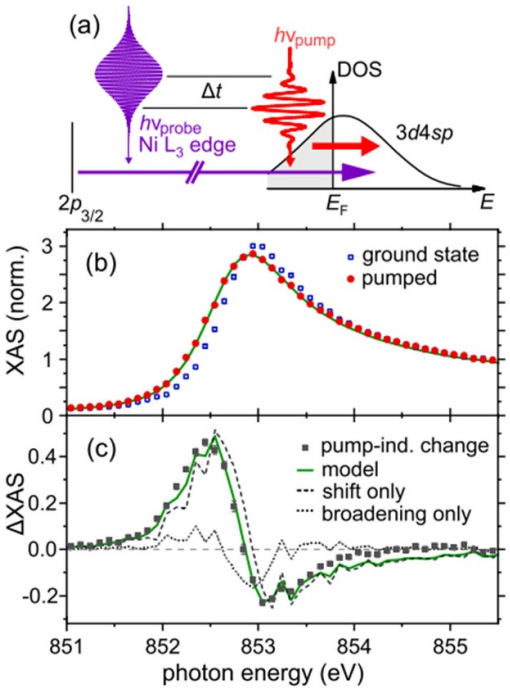

Figure 9. (a) Pump-probe scheme, with transient changes to the 3*d*4*sp* bands and their occupation induced by 1.5 eV excitation (indicated in red) probed by Ni L_3 edge tr-XAS. (b) Ground state (blue squares) and pumped (red circles) XAS at 0.4 ps pump-probe delay. (c) Transient change ΔXAS with modeling (green) by a combined spectral shift (dashed) and broadening (dotted line). [35] (2023), reprinted by permission of the publisher (Taylor & Francis Ltd, www.tandfonline.com).

spin–orbit interaction, fails to describe the pump-induced change ΔXAS. Only when local electronic correlations of the 3*d* states, in the form of a Hubbard *U*, are taken into account as well [35] do the TDDFT calculations agree with the experimental ΔXAS, see figure 10. With this comparison, the two processes behind the transient XAS redshift respectively broadening can be identified as band structure changes due to local correlations respectively electron population changes. Note that the high data quality achieved with the BOZ setup [31] described in section 2.3.2 makes this direct comparison to ab initio theory possible. This finding demonstrates the identification of the role of local correlations of the 3*d* orbitals in the ultrafast demagnetization of Ni and thereby reveals the previously mostly neglected influence of electronic correlations on the femtosecond electron and spin dynamics in transition metal ferromagnets.

Having established that the influence of electronic correlations in optically induced dynamics can be identified with tr-XAS, the next section 4.3 will move to a material with a stronger prominence of electronic correlations in its properties, namely the charge transfer insulator NiO.

4.3. Optically induced charge transfer dynamics in correlated transition metal oxides

4.3.1. Motivation

The material class of transition metal oxides has a high relevance for technological applications but also showcases fundamental physics of electronic correlations and many-body excitations. For advancing the fundamental understanding of the properties of this material class, a deeper insight into the processes after optical excitation is required. Of interest are the charge carrier excitation and relaxation as well as long-living, or even metastable, states which develop after optical excitation and exhibit properties that are different from the ground state and cannot be generated through e.g. thermal pathways [14]. One possibility to induce such states is photodoping, i.e. the generation of excited electrons and holes under resonant optical excitation [15].

NiO is employed as a model system for characterizing the non-equilibrium state after photodoping in a strongly correlated transition metal oxide. Due to local electronic correlations, the 3*d* states split into lower Hubbard band and UHB. Depending on the energetic position of the ligand (oxygen) 2*p* band, the oxide can be classified as a Mott-Hubbard or charge transfer insulator. NiO is thus a charge transfer insulator [131, 132], in which the direct band gap (optical gap) is given by transitions from O 2*p* states to the UHB [133]. The simplified DOS of NiO is shown in figure 11(a).

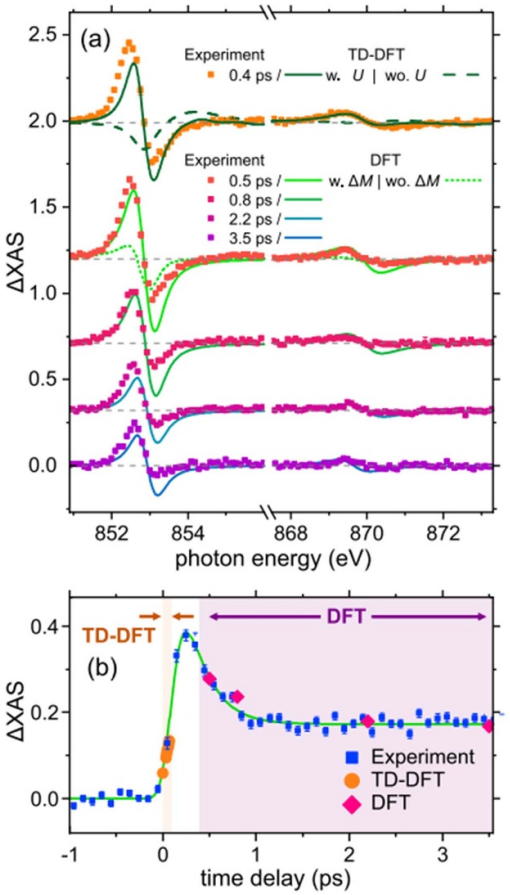

Figure 10. (a) Measured (markers) and calculated (solid lines) ΔXAS at the indicated pump-probe delays, including TDDFT calculations without U (dashed) respectively DFT calculations without demagnetization ΔM (dotted line). (b) Measured ΔXAS at 852.72 eV (blue squares) in comparison with values extracted from TDDFT (orange circles) respectively DFT calculations (pink diamonds). [35] (2023), reprinted by permission of the publisher (Taylor & Francis Ltd, www.tandfonline.com).

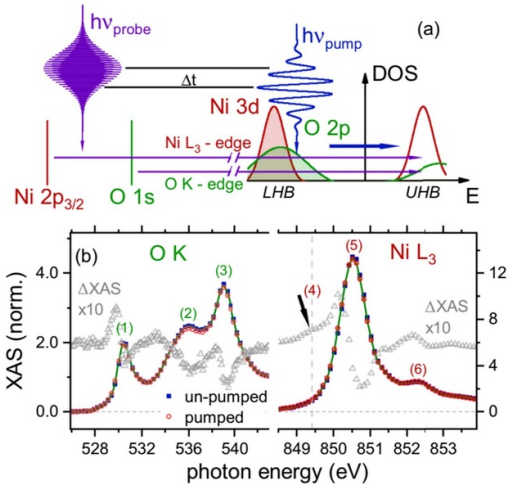

Figure 11. (a) Schematic depiction of NiO density of states (DOS) with resonant pump, tr-XAS probe experiment at the Ni L_3 and O K edges. (b) Ground state (blue squares) and pumped (red circles) XAS at the indicated absorption edges at 0.5 ps pump-probe delay, with the magnified, vertically offset pump-induced change ΔXAS (gray triangles). Green lines are fits to extract the spectral shift and broadening. Reprinted (figure) with permission from [37], Copyright (2024) by the American Physical Society.

Previous pump-probe experiments on NiO have mostly focused on sub-gap excitation [81, 82]. In the case of resonant, above-gap excitation the charge carriers were found to relax via Hund excitations on few fs timescales [133]. This relaxation of the initial charge transfer excitation is followed by polaron formation on a ps timescale [117]. Strikingly, for a comparatively simple transition metal oxide with

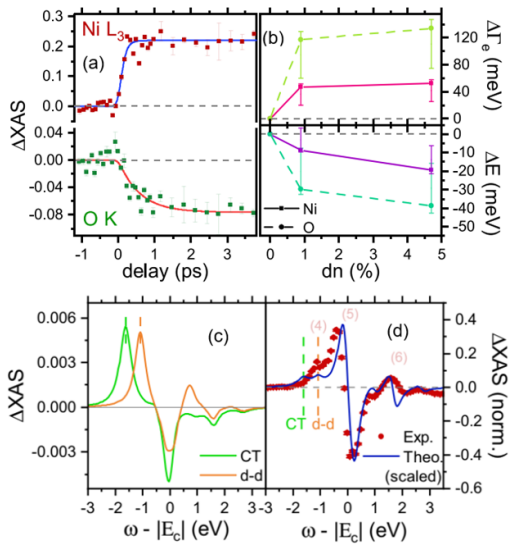

Figure 12. (a) Time dependence of ΔXAS for photodoped carrier density $dn = 4.7\%$ and (b) spectral broadening $\Delta\Gamma$ respectively shift ΔE for increasing dn. (c) Ni L_3 ΔXAS calculated by non-thermal multiplet ligand field theory for charge transfer (CT) and $d-d$ excitations, (d) scaled for comparison with experimental data at 0.25 ps (red circles). Reprinted (figure) with permission from [37], Copyright (2024) by the American Physical Society.

strong electronic correlations like NiO, that is well-investigated in the ground state, there are still significant gaps in the understanding of optically induced non-equilibrium states. Time-resolved XAS probes the unoccupied electronic structure while the element sensitivity of this method also distinguishes the dynamics at the oxygen ligand and transition metal sites [37]. The high data quality of this experiment is made possible by the recently implemented instrumentation at European XFEL [31].

4.3.2. Results and discussion

In order to induce photodoping, 37 nm thick NiO films grown by MBE on Si_3N_4 substrates [37] are resonantly excited across the direct band gap with a photon energy of 4.7 eV (wavelength 266 nm). This optical transition corresponds to the excitation across the charge transfer gap from oxygen 2*p* to nickel 3*d* states [133], see figure 11(a). The pump pulse thus generates holes in the ligand orbitals and increased electronic occupation on the transition metal sites.

The resulting dynamics are probed in an element-sensitive manner through tr-XAS [37], see figure 11(a). The O *K* and Ni L_3 edges both transiently shift to lower photon energies, see figure 11(b). Both edges show a transient broadening as well. Shift and broadening are quantified through fits as used in [35] (compare section 4.2). The results are displayed in figure 12(a): Depending on the absorption edge and amount of photodoping, the transient redshift lies in the range of 20–40 meV, while the spectra are transiently broadened by about 40–140 meV. These changes evolve to their maximum amount within < 1 ps and then persist for several ps practically unchanged, see figure 12(a).

A comparison with dynamical mean field theory (DMFT) calculations links the transient redshift to the underlying physical processes. Using a minimal model for a charge transfer insulator, namely the Emery or $d-p$ model [37], the reaction of the main XAS absorption peak at the Ni L_3 edge to photodoping is simulated. The calculations reproduce the transient redshift seen in the experiment, with a similar magnitude in range of several 10 meV for similar amounts of photodoping. The photodoping-induced shift of the spectrum can now be assigned to local and non-local electronic correlations, meaning modification of the electronic screening at the Ni sites respectively Coulomb interaction between photodoped electrons in the transition metal orbitals and holes in the oxygen (ligand) orbitals. The latter effect is termed a Hartree shift [37].

In addition to the transient redshift, a Ni L_3 pre-edge feature is visible on < 1 ps timescales, see figure 12(d). Assigning this transient fine structure requires a more material-specific theory. While the $d-p$ model employed in the DMFT calculations captures the main transient feature, i.e. a Coulomb-interaction mediated spectral shift, it is merely a minimal model for a generic charge transfer insulator and consequently the calculated XAS does not show fine structure specific to NiO. Therefore, multiple ligand field theory with non-thermal occupations is employed [37]. Through comparison with the calculation of the resulting XAS features from multiplet excitations of charge transfer and $d-d$ character, figure 12(c), the pre-edge feature can be assigned to $d-d$ excitations, see figure 12(d). It is separated

from the Coulomb interaction induced redshift spectrally and by its time dependence. Compared to the long-living spectral shifts discussed above, the multiplet feature already relaxes on 1–3 ps time scales [37]. Overall, these results demonstrate the identification of transient energy shifts due to Coulomb interaction and their separation from local multiplet occupations resulting from resonant photoexcitation, i.e. photodoping, of the prototypical charge transfer insulator NiO by femtosecond time-resolved XAS and complementary theoretical calculations.

Since the transient redshift persists on timescales of many ps, compare figure 12, it is likely that this long-living state involves not just the electronic but also the lattice degree of freedom. Corresponding lattice excitations are incoherent lattice motion due to electron–phonon coupling as well as polarons, which are known to form in transition metal oxides after both chemical doping and resonant optical excitation, i.e. photodoping [117]. Specifically for NiO polaron formation has been observed on 1–2 ps timescales [117]. The role of lattice excitations can be substantiated by an analysis of the transient broadening, in particular at the O *K* edge of NiO, see figure 12. A comparison with tr-XAS at the O *K* edge of MgO discussed in section 4.1 is instructive. Here, a similar transient broadening was observed and linked to lattice excitation [24, 30]. Consequently, the transient broadening at the O *K* edge of approximately 100 meV is most likely linked to polaron formation, which involves excitation of longitudinal optical phonons [117].

In addition, the analysis of long-living effects persisting beyond the repetition rate of stroboscopic tr-XAS [38] (see section 2.3.2) allows to substantiate the identification of polaron formation. Both the Ni L_{23} and O *K* edges show a persistent broadening, which builds up in a non-linear fashion and then saturates with increasing number of pump pulses in the pulse train of the FEL, i.e. cumulative excitation density. This behavior is distinctly different from the linear increase observed in metallic Ni films [31, 38], which was linked to lattice heating. Together with the known extremely long lifetimes of polarons on the order of ns to μs [134], the persistent XAS changes can thus be interpreted as trapping of excited charge carriers by polarons, which saturates at the Mott limit [135].

5. Conclusions

Femtosecond time-resolved XAS makes it possible to gain new insights into ultrafast charge and energy transfer dynamics in solids and at interfaces through element-sensitivity as well as the characteristic shape and time-dependence of transient spectral features, as summarized in figure 4 respectively figure 5 for electronic respectively lattice excitations. In particular, the improved energy and temporal resolution of tr-XAS at FELs compared to synchrotron Femtoslicing sources allows a direct comparison with ab initio theoretical calculations, which is highly beneficial for revealing if certain physical processes are relevant for the dynamics under investigation.

The three different material systems reviewed here show that tr-XAS can characterize non-equilibrium states in metals, insulators and metal/insulator heterostructures by analyzing the transient electronic structure via time-dependent spectral features. A particular focus lies on correlation induced band structure modifications either through a cooperation of ultrafast spin dynamics, mediated by spin–orbit interaction, and local electronic correlations in the transition metal ferromagnet Ni [35], or through local modification of screening and non-local Coulomb interaction between photodoped electrons and holes in the charge transfer insulator NiO [37]. Such electronic excitations are distinguished from lattice excitations via different transient spectral signatures, namely a shift versus broadening of the near-edge fine structure extracted through fitting procedures. The sensitivity to lattice excitations was exploited to reveal sub-picosecond energy transfer across the interfaces of Fe/MgO metal/insulator heterostructures by coupling of hot electrons in Fe to hybrid interface phonon modes [24].

Overall, technological and methodological advances in tr-XAS at FELs increasingly allow to utilize the full spectral information also with fs time resolution. Consequently, future experiments will be able to exploit a systematic variation of x-ray, optical and/or material parameters and increasingly move from model systems, as discussed in this overview, to more complex materials and heterostructures.

6. Outlook

In the three examples discussed in section 4, all spectra were acquired with linear x-ray polarization. However, helical undulators for generating circular polarization are available at both Femtoslicing sources and FELs, offering the possibility to probe spin-dependent dynamics and transient magnetic order. While time-resolved XMCD has in fact been widely used to analyze ultrafast magnetization dynamics in ferro-

and ferrimagnets [4, 6, 25, 29], an extension to femtosecond dynamics of antiferromagnetic materials through XMLD is so far much rarer. Chiral dichroism can further be employed to address the dynamics of chiral materials or transient chiral order induced by THz pumping [136]. Time-resolved XMCD will also benefit from the improved time- and energy resolution as well as data quality made possible by FELs, for example with respect to the application of sum rules for a quantitative analysis for spin- and orbital momenta.

A further recent development enabled by extreme x-ray intensities at FELs is time-resolved resonant inelastic x-ray scattering in solids, as for example demonstrated in iridates [137, 138], Tb [53], graphite [139] and NiO [140]. Pushed forward by continuing improvements in the spectral resolution, this technique makes it possible to directly analyze the temporal evolution of electronic, spin and vibrational excitations.

I would also like to briefly highlight two methodological developments in recent years: Laboratory-based sources of ultrashort x-ray pulses pave the way toward greater access to tr-XAS, while the extreme x-ray intensities generated at FELs enable time-resolved non-linear x-ray spectroscopy.

6.1. Laboratory-based sources

A practical drawback to tr-XAS at large scale facilities, i.e. synchrotron Femtoslicing sources and FELs, is limited access to beamtime, as these facilities generally only accommodate a single or few experiments at any given time. With the observation of high harmonic generation (HHG), a laboratory-based alternative increasingly becomes available. The interaction of high intensity visible or infrared femtosecond laser pulses with nobles gases induces the emission of ultrashort vacuum ultraviolet pulses, whose energy can extend up to keV if mid-infrared drivers are used [141]. Since a fs laser serves as driver for HHG, it is straightforward to use part of the beam as a pump pulse for tr-XAS with intrinsic temporal synchronization. The use of such HHG sources for resonant time-resolved absorption spectroscopy and magneto-optical techniques in the extreme ultraviolet and even soft x-range range is by now fairly well-established [142].

6.2. Time-resolved non-linear XAS

In the visible and infrared spectral range, non-linear spectroscopy methods such as SHG and sum-frequency generation (SFG) are established techniques. In particular, SHG spectroscopy provides intrinsic surface- and interface-sensitivity in centrosymmetric materials, as SHG vanishes under spatial inversion symmetry and thus only occurs where at interfaces where spatial inversion symmetry is broken. Magnetic contrast in this technique is used to analyze ferro- and antiferromagnetic order, and it can be further be implemented as the probe in fs time-resolved pump-probe experiments [8]. As seen in section 4.1, tr-XAS is able to address dynamics at interfaces even if linear x-ray absorption is in general a bulk-sensitive probe. As a next step, it will be beneficial to combine the element- and chemical sensitivity of XAS with interface-sensitivity provided by non-linear spectroscopy through x-ray SHG spectroscopy.

X-ray SHG and SFG have recently been demonstrated, among other non-linear effects in the x-ray range [42]. For example, as described in section 2.4, non-linear effects in L_3 edge x-ray absorption spectra of Ni at very high x-ray fluences were identified [41]. Combining non-linear XAS and pump-probe experiments will take advantage of the parameters offered by XFELs, namely the high x-ray intensities combined with ultrashort pulse duration, necessary to drive non-linear effects and simultaneously ensure femtosecond time resolution.

Acknowledgments

While I cannot acknowledge every collaborator involved in the work reviewed here individually, I would like to thank everyone for their contribution, without which gaining new insights from time-resolved x-ray absorption spectroscopy would have not been possible. First and foremost, I would like to thank the PhD graduates Lea Kämmerer, Tobias Lojewski and Nico Rothenbach as well as my experimental collaborators within the SFB 1242, Katharina Ollefs, Uwe Bovensiepen, Klaus Sokolowski-Tinten and Heiko Wende. I would further like to thank the beamline scientists at the Femtoslicing facility of BESSY II as well as the SCS instrument of European XFEL, in particular Loic Le Guyader and Andreas Scherz. Finally, I would like to acknowledge the very fruitful collaborations between experiment and theory and thank in particular Rossitza Pentcheva, Markus E Gruner, Mohamed F Elhanoty, Olle Eriksson, Denis Golez, Martin Eckstein and Philipp Werner.

Funded by the Deutsche Forschungsgemeinschaft (DFG, German Research Foundation) - Project-ID 278162697 - SFB 1242.

Data availability statement

No new data were created or analysed in this study.

Author contribution

A Eschenlohr 0000-0002-0814-3511
Conceptualization (lead), Funding acquisition (lead), Writing – original draft (lead)

References

[1] Bauer M, Marienfeld A and Aeschlimann M 2015 *Prog. Surf. Sci.* **90** 319
[2] Melnikov A, Razdolski I, Wehling T O, Papaioannou E T, Roddatis V, Fumagalli P, Aktsipetrov O, Lichtenstein A I and Bovensiepen U 2011 *Phys. Rev. Lett.* **107** 076601
[3] Beyazit Y, Beckord J, Zhou P, Meyburg J P, Kühne F, Diesing D, Ligges M and Bovensiepen U 2020 *Phys. Rev. Lett.* **125** 076803
[4] Eschenlohr A 2020 *J. Phys.: Condens. Matter* **33** 013001
[5] Battiato M, Carva K and Oppeneer P M 2010 *Phys. Rev. Lett.* **105** 027203
[6] Kirilyuk A, Kimel A V and Rasing T 2010 *Rev. Mod. Phys.* **82** 2731
[7] Krieger K, Dewhurst J K, Elliott P, Sharma S and Gross E K U 2015 *J. Chem. Theory Comput.* **11** 4870
[8] Chen J, Bovensiepen U, Eschenlohr A, Müller T, Elliott P, Gross E K U, Dewhurst J K and Sharma S 2019 *Phys. Rev. Lett.* **122** 067202
[9] Hohlfeld J, Wellershoff S-S, Güdde J, Conrad U, Jähnke V and Matthias E 2000 *Chem. Phys.* **251** 237
[10] Anisimov S I, Kapeliovich B L and Perel'man T L 1974 *JETP* **39** 375 (available at: https://jetp.ras.ru/cgi-bin/dn/e_039_02_0375.pdf)
[11] Beaurepaire E, Merle J-C, Daunois A and Bigot J-Y 1996 *Phys. Rev. Lett.* **76** 4250
[12] Maldonado P, Carva K, Flammer M and Oppeneer P M 2017 *Phys. Rev.* B **96** 174439
[13] Giannetti C, Capone M, Fausti D, Fabrizio M, Parmigiani F and Mihailovic D 2016 *Adv. Phys.* **65** 58
[14] de la Torre A, Kennes D M, Claassen M, Gerber S, McIver J W and Sentef M A 2021 *Rev. Mod. Phys.* **93** 041002
[15] Murakami Y, Gole D, Eckstein M and Werner P 2025 *Rev. Mod. Phys.* **97** 035001
[16] De Groot F 2001 *Chem. Rev.* **101** 1779
[17] Wende H 2004 *Rep. Prog. Phys.* **67** 2105
[18] Chantler C T, Bunker G, D'Angelo P and Diaz-Moreno S 2024 *Nat. Rev. Methods Primers* **4** 89
[19] Fischer P and Ohldag H 2015 *Rep. Prog. Phys.* **78** 094501
[20] Vaz C A F *et al* 2025 *Nat. Rev. Methods Primers* **5** 27
[21] Sanson A 2021 *Microstructures* **1** 2021004
[22] Holldack K, Kachel T, Khan S, Mitzner R and Quast T 2005 *Phys. Rev. Spec. Top. Accel. Beams* **8** 040704
[23] Holldack K *et al* 2014 *J. Synchrotron Radiat.* **21** 1090
[24] Rothenbach N *et al* 2019 *Phys. Rev.* B **100** 174301
[25] Stamm C *et al* 2007 *Nat. Mater.* **6** 740
[26] Boeglin C, Beaurepaire E, Halté V, López-Flores V, Stamm C, Pontius N, Dürr H A and Bigot J-Y 2010 *Nature* **465** 458
[27] Stamm C, Pontius N, Kachel T, Wietstruk M and Dürr H A 2010 *Phys. Rev.* B **81** 104425
[28] Eschenlohr A, Battiato M, Maldonado P, Pontius N, Kachel T, Holldack K, Mitzner R, Föhlisch A, Oppeneer P M and Stamm C 2013 *Nat. Mater.* **12** 332
[29] Radu I *et al* 2011 *Nature* **472** 205
[30] Rothenbach N *et al* 2021 *Phys. Rev.* B **104** 144302
[31] Le Guyader L *et al* 2023 *J. Synchrotron Radiat.* **30** 284
[32] Seddon E *et al* 2017 *Rep. Prog. Phys.* **80** 115901
[33] Gahl C *et al* 2008 *Nat. Photon.* **2** 165
[34] Hartmann N *et al* 2014 *Nat. Photon.* **8** 706
[35] Lojewski T *et al* 2023 *Mater. Res. Lett.* **11** 655
[36] Kämmerer L *et al* 2024 *ACS Nano* **18** 34596
[37] Lojewski T *et al* 2024 *Phys. Rev.* B **110** 245120
[38] Lojewski T *et al* 2024 Analysis of long-lived effects in high-repetition-rate stroboscopic transient x-ray absorption experiments on thin films (https://doi.org/10.48550/arXiv.2412.05151)
[39] Schlotter W *et al* 2020 arXiv:2006.13968
[40] Porro M *et al* 2010 *Nucl. Instrum. Methods Phys. Res.* A **624** 509
[41] Engel R Y *et al* 2023 *Struct. Dyn.* **10** 054501
[42] Chergui M, Beye M, Mukamel S, Svetina C and Masciovecchio C 2023 *Nat. Rev. Phys.* **5** 578
[43] Higley D J *et al* 2019 *Nat. Commun.* **10** 5289
[44] Kraus P M, Zürch M, Cushing S K, Neumark D M and Leone S R 2018 *Nat. Rev. Chem.* **2** 82
[45] Kobayashi Y and Leone S R 2022 *J. Chem. Phys.* **157** 180901
[46] Carlson D R, Bandaranayake S and Ramasesha K 2025 *Annu. Rev. Phys. Chem.* **77** 129–52
[47] Wörner H J and Wolf J-P 2025 *Nat. Rev. Chem.* **9** 185
[48] Kachel T, Pontius N, Stamm C, Wietstruk M, Aziz E F, Dürr H A, Eberhardt W and de Groot F M F 2009 *Phys. Rev.* B **80** 092404

[49] Wach A *et al* 2025 *Nat. Commun.* **16** 2274
[50] Cho B *et al* 2011 *Phys. Rev. Lett.* **106** 167601
[51] Mahieu B, Jourdain N, Ta Phuoc K, Dorchies F, Goddet J-P, Lifschitz A, Renaudin P and Lecherbourg L 2018 *Nat. Commun.* **9** 3276
[52] Lee J-W *et al* 2021 *Phys. Rev. Lett.* **127** 175003
[53] Thielemann-Kühn N *et al* 2024 *Phys. Rev. Lett.* **10** eadk9522
[54] Amrhein T, Salantur B, Püttner R, Pontius N, Holldack K, Wang R-P, Schüßler-Langeheine C, Weinelt M and Thielemann-Kühn N 2025 arXiv:2504.19630
[55] Zürch M *et al* 2017 *Nat. Commun.* **8** 15734
[56] Sidiropoulos T, Di Palo N, Rivas D, Summers A, Severino S, Reduzzi M and Biegert J 2023 *Nat. Commun.* **14** 7407
[57] Cannelli O *et al* 2021 *J. Am. Chem. Soc.* **143** 9048
[58] Santomauro F G *et al* 2015 *Sci. Rep.* **5** 14834
[59] Carneiro L M, Cushing S K, Liu C, Su Y, Yang P, Alivisatos A P and Leone S R 2017 *Nat. Mater.* **16** 819
[60] Jiang C-M, Baker L R, Lucas J M, Vura-Weis J, Alivisatos A P and Leone S R 2014 *J. Phys. Chem.* C **118** 22774
[61] Vura-Weis J, Jiang C-M, Liu C, Gao H, Lucas J M, De Groot F M, Yang P, Alivisatos A P and Leone S R 2013 *J. Phys. Chem. Lett.* **4** 3667
[62] Ismail A S *et al* 2020 *Phys. Chem. Chem. Phys.* **22** 2685
[63] Uemura Y *et al* 2022 *J. Phys. Chem. Lett.* **13** 4207
[64] Park S H *et al* 2022 *Nat. Commun.* **13** 2531
[65] Uemura Y *et al* 2021 *J. Phys. Chem.* C **125** 7329
[66] Lazemi M *et al* 2025 *Adv. Mater.* **37** 2502932
[67] Rossi T C, Dykstra C P, Haddock T N, Wallick R, Burke J H, Gentle C M, Doumy G, March A M and Van Der Veen R M 2021 *Nano Lett.* **21** 9534
[68] Rossi T C *et al* 2025 *Commun. Mater.* **6** 191
[69] Cistaro G, Plaja L, Martín F and Picón A 2021 *Phys. Rev. Res.* **3** 013144
[70] Yan J, Er H, Dang W, Ren J, Chen C, Ren D and Dong F 2025 *Phys. Rev.* B **112** 205410
[71] Yan J, Zhu C, Zhang R, Zhao X and Dong F 2026 *Phys. Rev.* A **113** 013123
[72] Mosquera J F P, Cistaro G, Malakhov M, Pisanty E, Dauphin A, Plaja L, Chacón A, Lewenstein M and Picón A 2024 *Rep. Prog. Phys.* **87** 117901
[73] Yamada S, Yabana K and Otobe T 2023 *Phys. Rev.* B **108** 035404
[74] Quintela M F C M, Sá M, Uría-Álvarez A J, Malakhov M, Cistaro G, Quereda J, Palacios J J and Picón A 2025 *Phys. Rev. Res.* **7** 043265
[75] Britz A *et al* 2021 *Struct. Dyn.* **8** 014501
[76] Attar A R *et al* 2020 *ACS Nano* **14** 15829
[77] Chang H-T, Guggenmos A, Chen C T, Oh J, Géneaux R, Chuang Y-D, Schwartzberg A M, Aloni S, Neumark D M and Leone S R 2021 *Phys. Rev.* B **104** 064309
[78] Oh J, Chang H-T, Chen C T, Aloni S, Schwartzberg A and Leone S R 2023 *J. Phys. Chem.* C **127** 5004
[79] Heinrich T, Chang H-T, Zayko S, Rossnagel K, Sivis M and Ropers C 2023 *Phys. Rev.* X **13** 021033
[80] Baykusheva D R *et al* 2022 *Phys. Rev.* X **12** 011013
[81] Grnäs O *et al* 2022 *Phys. Rev. Res.* **4** L032030
[82] Wang X *et al* 2022 *Faraday Discuss.* **237** 300
[83] Lee J-S *et al* 2026 *Phys. Rev.* X **16** 011064
[84] Vura-Weis J 2025 *Annu. Rev. Phys. Chem.* **76** 455
[85] Bergeard N, López-Flores V, Halte V, Hehn M, Stamm C, Pontius N, Beaurepaire E and Boeglin C 2014 *Nat. Commun.* **5** 3466
[86] Chen C, Idzerda Y, Lin H-J, Smith N, Meigs G, Chaban E, Ho G, Pellegrin E and Sette F 1995 *Phys. Rev. Lett.* **75** 152
[87] Radu I *et al* 2015 *SPIN* **05** 1550004
[88] Ryan S A *et al* 2023 *Sci. Adv.* **9** eadi1428
[89] Wietstruk M, Melnikov A, Stamm C, Kachel T, Pontius N, Sultan M, Gahl C, Weinelt M, Dürr H A and Bovensiepen U 2011 *Phys. Rev. Lett.* **106** 127401
[90] Eschenlohr A, Sultan M, Melnikov A, Bergeard N, Wieczorek J, Kachel T, Stamm C and Bovensiepen U 2014 *Phys. Rev.* B **89** 214423
[91] Thielemann-Kühn N, Schick D, Pontius N, Trabant C, Mitzner R, Holldack K, Zabel H, Föhlisch A and Schüßler-Langeheine C 2017 *Phys. Rev. Lett.* **119** 197202
[92] Eschenlohr A, Persichetti L, Kachel T, Gabureac M, Gambardella P and Stamm C 2017 *J. Phys.: Condens. Matter* **29** 384002
[93] Gupta D *et al* 2025 *Nat. Commun.* **16** 3097
[94] Kumberg I *et al* 2020 *Phys. Rev.* B **102** 214418
[95] Gördes J, Kumberg I, Awsaf C S, Walter M, Shinwari T, Thakur S, Sharma S, Schüßler-Langeheine C, Pontius N and Kuch W 2025 *Phys. Rev.* B **112** 104442
[96] Sharma S, Gill D, Krishna J, Harris-Lee E, Dewhurst J K and Shallcross S 2026 *Nat. Commun.* **17** 5069
[97] Baker A, Figueroa A, Collins-McIntyre L, Van Der Laan G and Hesjedal T 2015 *Sci. Rep.* **5** 7907
[98] Tsuyama T, Chakraverty S, Macke S, Pontius N C, Hwang H Y, Tokura Y and Wadati H 2016 *Phys. Rev. Lett.* **116** 256402
[99] Golias E *et al* 2021 *Phys. Rev. Lett.* **126** 107202
[100] Awsaf C S *et al* 2026 *Phys. Rev. Lett.* **136** 126705
[101] Malinowski G, Bergeard N, Hehn M and Mangin S 2018 *Eur. Phys. J.* B **91** 98
[102] Kimel A *et al* 2022 *J. Phys. D: Appl. Phys.* **55** 03765500
[103] Wadati H, Yamamoto K and Yamagami K 2026 *X-Ray Spectrom.* (https://doi.org/10.1002/xrs.70107)
[104] Chergui M and Collet E 2017 *Chem. Rev.* **117** 11025
[105] Izquierdo M *et al* 2014 *Phys. Rev.* B **90** 235128
[106] Izquierdo M, Karolak M, Prabhakaran D, Boothroyd A T, Scherz A O, Lichtenstein A and Molodtsov S L 2019 *Commun. Phys.* **2** 8
[107] Londo S, Biswas S, Pinchuk I V, Boyadzhiev A, Kawakami R K and Baker L R 2022 *J. Phys. Chem.* C **126** 2669
[108] Burke J H *et al* 2026 *Inorg. Chem.* **65** 2136
[109] Elsaesser T and Woerner M 2014 *J. Chem. Phys.* **140** 020901

[110] Buzzi M, Först M, Mankowsky R and Cavalleri A 2018 *Nat. Rev. Mater.* **3** 299
[111] Johnson S L and Staub U 2025 *npj Quantum Mater.* **10** 78
[112] Filippetto D, Musumeci P, Li R K *et al* 2022 *Rev. Mod. Phys.* **94** 045004
[113] Van Der Veen R M *et al* 2009 *Angew. Chem.* **121** 2749
[114] Bressler C and Chergui M 2010 *Annu. Rev. Phys. Chem.* **61** 263
[115] Katz J E, Zhang X, Attenkofer K, Chapman K W, Frandsen C, Zarzycki P, Rosso K M, Falcone R W, Waychunas G A and Gilbert B 2012 *Science* **337** 1200
[116] Pelatti S *et al* 2025 *Adv. Electron. Mater.* **11** e00429
[117] Biswas S, Husek J, Londo S and Baker L R 2018 *J. Phys. Chem. Lett.* **9** 5047
[118] Kumar V, Dharmadhikari A K and Biswas S 2026 *J. Phys. Chem. Lett.* **17** 2499
[119] Jal E, López-Flores V, Pontius N, Ferté T, Bergeard N, Boeglin C, Vodungbo B, Lüning J and Jaouen N 2017 *Phys. Rev.* B **95** 184422
[120] Chardonnet V *et al* 2021 *Struct. Dyn.* **8** 034305
[121] Petti D, Cantoni M, Rinaldi C and Bertacco R 2011 *J. Phys.: Conf. Ser.* **292** 012010
[122] Windsor Y W *et al* 2026 *Adv. Sci.* e77058
[123] Rivera P, Yu H, Seyler K L, Wilson N P, Yao W and Xu X 2018 *Nat. Nanotechnol.* **13** 1004
[124] Regan E C, Wang D, Paik E Y, Zeng Y, Zhang L, Zhu J, MacDonald A H, Deng H and Wang F 2022 *Nat. Rev. Mater.* **7** 778
[125] Battiato M, Carva K and Oppeneer P M 2012 *Phys. Rev.* B **86** 024404
[126] Koopmans B, Malinowski G, Dalla Longa F, Steiauf D, Fähnle M, Roth T, Cinchetti M and Aeschlimann M 2010 *Nat. Mater.* **9** 259
[127] Eich S *et al* 2017 *Sci. Adv.* **3** e1602094
[128] Acharya S R, Turkowski V, Zhang G and Rahman T S 2020 *Phys. Rev. Lett.* **125** 017202
[129] Koopmans B, Van Kampen M, Kohlhepp J and De Jonge W 2000 *Phys. Rev. Lett.* **85** 844
[130] Guidoni L, Beaurepaire E and Bigot J-Y 2002 *Phys. Rev. Lett.* **89** 017401
[131] Zaanen J, Sawatzky G A and Allen J W 1985 *Phys. Rev. Lett.* **55** 418
[132] Kunes J, Anisimov V I, Lukoyanov A V and Vollhardt D 2007 *Phys. Rev.* B **75** 165115
[133] Gillmeister K, Golez D, Chiang C-T, Bittner N, Pavlyukh Y, Berakdar J, Werner P and Widdra W 2020 *Nat. Commun.* **11** 4095
[134] Foglia L, Vempati S, Tanda Bonkano B, Gierster L, Wolf M, Sadofev S and Stähler J 2019 *Struct. Dyn.* **6** 034501
[135] Zhang H *et al* 2023 *ACS Energy Lett.* **8** 420
[136] Basini M, Pancaldi M, Wehinger B, Udina M, Unikandanunni V, Tadano T, Hoffmann M C, Balatsky A V and Bonetti S 2024 *Nature* **628** 534
[137] Dean M P *et al* 2016 *Nat. Mater.* **15** 601
[138] Mazzone D G *et al* 2021 *Proc. Natl. Acad. Sci. U.S.A.* **118** e2103696118
[139] Malvestuto M *et al* 2026 *Nat. Commun.* **17** 1158
[140] Merzoni G *et al* 2025 arXiv:2504.16653
[141] Popmintchev T *et al* 2012 *Science* **336** 1287
[142] Yackovich M A, Locklear M W and Liu H 2023 *J. Mater. Chem.* C **11** 12128